Glutamate-Induced Deregulation of Krebs Cycle in Mitochondrial Encephalopathy Lactic Acidosis Syndrome Stroke-Like Episodes (MELAS) Syndrome Is Alleviated by Ketone Body Exposure

Sophie Belal, David Goudenège, Cinzia Bocca, Florent Dumont, Juan Manuel Chao de la Barca, Valérie Desquiret-Dumas, Naïg Gueguen, Guillaume Geffroy, Rayane Benyahia, Selma Kane, et al.

MELAS syndrome causes glutamate and tricarboxylic acid cycle dysfunctions alleviated by ketone body treatment

Sophie Belal[1], David Goudenege[1,2], Cinzia Bocca[1], Florent Dumont[3], Juan Manuel Chao De La Barca[1,2], Valerie Desquiret-Dumas[1,2], Naig Gueguen[1,2], Guillaume Geffroy[1], Rayane Benyahia[1], Selma Kane[1], Salim Khiati[1], Celine Bris[1,2], Tamas Aranyi[4], Daniel Stockholm[5,6], Aurore Inisan[1], Aurelie Renaud[1], Magalie Barth[2], Gilles Simard[2], Pascal Reynier[1,2], Franck Letournel[7], Guy Lenaers[1], Dominique Bonneau[1,2], Arnaud Chevrollier[1], Vincent Procaccio[1,2]

[1]Univ Angers, CHU Angers, INSERM, CNRS, MITOVASC, SFR ICAT, F-49000 Angers, France
[2]Biochemistry and Genetics Department, University Hospital of Angers, France
[3]Signalling and Cardiovascular Pathophysiology, INSERM UMR-S 1180, University of Paris-Saclay, Châtenay-Malabry, France
[4]Research centre for natural science, Hungarian Academy of sciences - Budapest - Hungary
[5]Ecole Pratique des Hautes Etudes, PSL Research University, Paris, France
[6]Centre de Recherche Saint-Antoine, UMRS-938, Sorbonne Université, INSERM, F-75012 Paris, France
[7]UMR INSERM 1066 - CNRS 6021, MINT laboratory, University Hospital of Angers, Angers, France

To whom correspondence should be addressed: Prof. Vincent Procaccio M.D., Ph.D. Genetics Department, Angers University Hospital, 4 rue Larrey, 49933 Angers, France. Phone 33 2 41 35 78 54. Fax 33 2 41 35 58 83. E-mail: ViProcaccio@chu-angers.fr

Word count: 10156 words
Title: 14 words
Abstract: 228 words
64 References, 9 Figures, 2 Tables, 2 Supplemental Figures, 2 Supplemental Tables

Keywords: Mitochondrial diseases; mtDNA; MELAS syndrome; Multi-omics; Glutamate; Tricarboxylic acid cycle; NADH/NAD imbalance; Ketone body treatment;

ABSTRACT

The development of mitochondrial medicine is severely hampered by a lack of knowledge about the pathophysiological mechanisms underlying mitochondrial disorders as well as effective therapies targeting mitochondria. To better understand the Mitochondrial Encephalopathy Lactic Acidosis Syndrome Stroke-like episodes (MELAS) syndrome, neuronal cybrid cells, harboring different mutant loads of the m.3243A>G pathogenic variant in the mitochondrial DNA, were studied using an approach combining metabolomics and transcriptomics. Specific metabolomic signatures revealed that the glutamate pathway was strongly involved in the pathophysiology of MELAS syndrome and established a positive correlation between glutamate concentration and the m.3243A>G heteroplasmy level. Transcriptomic analyses in cells harboring 98% mutant load further revealed alterations in specific gene clusters, including those of the glutamate and gamma-aminobutyric acid (GABA) pathways as well as those of the tricarboxylic acid (TCA) cycle. These results were supported by an analysis of post-mortem brain tissue obtained from an individual with MELAS, confirming the dysregulation of the glutamate metabolic pathway. Exposure of MELAS cells to ketone bodies induced a significant reduction of glutamate level and improved mitochondrial functions, alleviating the accumulation of several intermediate metabolites of the TCA cycle witnessing NADH-redox imbalance. Thus, our integrated approach using a multi-omics strategy on MELAS cybrid cells, revealed new avenues to explain the mitochondrial energy failure, identifying glutamate as a biomarker of the disease, while indicating that ketogenic diet should be clinically tested in MELAS patients.

Introduction

Mitochondria, as the power plant of the cells, produce ATP through the oxidative phosphorylation (OXPHOS) process, located in the inner mitochondrial membrane (1). Mitochondrial diseases arise from pathogenic variants in mitochondrial DNA (mtDNA) or in nuclear genes that encode proteins essential for mitochondrial functions (2, 3). The mitochondrial genome encodes 22 transfer RNAs (tRNAs) and 2 ribosomal RNAs (rRNAs), required for the translation of 13 polypeptides, all included in the OXPHOS complexes (1).

One of the most commonly encountered mtDNA mutations involved in mitochondrial disorders is the m.3243A>G pathogenic variant in *MT-TL1*, which is responsible for the life-threatening MELAS syndrome (4), when present in high mutant loads. Although clinically heterogeneous, MELAS syndrome is characterized by a triad of symptoms including lactic acidosis, stroke like episodes before the age of 40, and encephalopathy (5). MELAS syndrome also includes a wide spectrum of additional features such as epilepsy, diabetes, exercise intolerance, myopathy, dementia and deafness (6).

The severity of MELAS syndrome is related to the m.3243A>G heteroplasmy level, reflecting the coexistence of wild type and mutant mtDNA copies (1, 3). The m.3243A>G variant affects the *MT-TL1* gene, encoding the $tRNA^{Leu(UUR)}$, leading to the alteration of its structure, stability, amino-acylation and codon recognition, thus reducing the efficiency of the mitochondrial translational machinery (7-9). MELAS is associated with multiple partial respiratory chain defects, particularly involving mitochondrial complex I and/or complex IV deficiencies (4, 10-12). However, complex I deficiency is often viewed as the key element of the disease (13-15). Additional rare pathogenic variants responsible for MELAS have been also identified in other genes encoding mitochondrial tRNA, affecting either the synthesis of proteins or NADH Dehydrogenase (ND) subunits (i.e. ND1, ND5 and ND6 subunits). These variants have been functionally validated by the reduction of

complex I activity in neuronal cellular models of MELAS (16, 17), further highlighting the crucial role of complex I deficiency in the pathophysiology of the disease (5, 18)

The considerable efforts made to better understand the pathophysiology of MELAS have so far not led to the discovery of effective specific therapies. (1, 11).

Several compounds have been used in individuals affected with MELAS including coenzyme Q10, L-arginine, and citrulline, but none of them have shown real clinical efficacy (1, 10, 11), particularly in alleviating the stroke-like episodes (19). Alternatively, ketogenic diet, which combines carbohydrate restriction and ketone bodies (KB) supplementation has been used for decades to treat drug-resistant epilepsies (20). This success has prompted testing of ketogenic diet to treat other severe neurological disorders including MELAS syndrome (21-23). In this regard, we have previously shown that long-term exposure to KB significantly improves complex I activity and assembly (21) in MELAS neuronal cybrids, in which there is a strong reduction of mitochondrial complex I activity and assembly identical to what is observed in fibroblasts and muscle biopsies obtained from MELAS patients (13, 16, 17, 24).

In order to thoroughly assess the consequences of the m.3243A>G MELAS variant, we used a multi-OMICS approach on MELAS mutant cybrid neuronal cells, to unravel the affected metabolic pathways and identify potential biomarkers. We then tested the effects of exposure to KB on the observed mitochondrial dysregulation.

RESULTS

A multi-OMIC approach highlights specific signatures in MELAS mutant cells. To gain insight into MELAS metabolic changes, a targeted metabolomic analysis quantifying a total of 188 metabolites, was carried out on cellular extracts from cybrid SHSY-5Y neuronal cells, harboring different m.3243A>G mutant load (i.e. 70%, 90% and 98%), compared to control cells. Unsupervised principal component analysis (PCA) of metabolomics data from parental cells (n=10) and cells harboring the MELAS mutation with different mutation loads (n=30), disclosed a clear segregation between mutant and non-mutant cells (Figure 1A) as well as between cells harboring different mutation loads (Figure 1B), validating the metabolomic analysis.

Compared to control cells, mutant cells harboring 70 to 98% mutant loads revealed a metabolic signature characterized by significant lower levels of 6 acylcarnitines (i.e. C0, C2, C4, C16, C18, C18:1) and 10 amino acids (i.e. alanine, glutamine, serine, lysine, proline, glycine, serotonine, spermine, arginine and taurine) (Figure 1C). Interestingly, arginine and taurine, 2 key amino acids already known to be involved in the pathophysiology of MELAS (27, 28), were significantly reduced in mutant cells. In addition, several phospholipids, lysophospholipids and sphingomyelins were significantly increased in mutant cells (Figure 1C). Interestingly, the comparison of the metabolic signature of MELAS cells harboring different mutant loads identified 10 amino acids (i.e. phenylalanine, tyrosine, valine, tryptophan, isoleucine, leucine, threonine, histidine, methionine and alpha-aminoadipic acid) which concentrations were significantly decreased between the 70% and 90% mutant cells, compared to 98% mutant cells (Figure 1D). Conversely, 14 metabolites, including 6 phosphocholines and lysophosphocholines, 8 amino acids (i.e. ornithine, acetyl ornithine, trans-4-hydroxyproline, aspartic acid, alanine, glutamine, glutamate and DOPA) were significantly increased in 98% mutant cells, compared to lower mutant loads (Figure 1D), thus pointing on highly specific changes in amino-acid and biogenic amine metabolite concentrations, according to the m.3243A>G heteroplasmy level.

*The level of intra cellular glutamate correlates positively with the heteroplasmy level and negatively with mitochondrial complex I activity.*Quantification of glutamate showed higher intracellular glutamate concentrations in MELAS mutant cells, reaching a 4-fold increase in cells containing 98% mutant load compared to control cells (Figure 2A). Furthermore, the intracellular glutamate concentration was positively correlated with the heteroplasmy level in mutant cells (Figure 2A) and was inversely proportional to the complex I activity related to mitochondrial citrate synthase (CS) activity (Figure 2B). Likewise, the intracellular glutamate concentration was increased by 55% in another cell type, 143B osteosarcoma cybrid cells carrying the m.3243A>G mutation with a 98% mutant load, compared to the 143B control cybrid cells (supplemental S1).

Next, we investigated for a relationship between the level of glutamate and the activity of complex I by exposing control cells during 15h to rotenone, a complex I inhibitor.

This experiment showed a 58.5% reduction in complex I activity compared to untreated cells, which was associated to a 245% increase of intracellular glutamate concentration, compared to untreated cells (Figure 2C and 2D). This suggests that the activity of mitochondrial complex I regulates the intracellular glutamate concentration.

In addition, the level of extracellular glutamate was also significantly increased in mutant cells with various mutant loads, compared to control cells (Figure 2E). Nevertheless, the extracellular glutamate concentration was lower in the 98% mutant cells compared to 70% and 90% mutant cells (Figure 2E).

Since glutamine is a precursor for the biosynthesis of glutamate, we next monitored the intracellular glutamate level in cells cultured with or without glutamine. We found a reduction in intracellular glutamate in control and 98% mutant cells grown in a glutamine-free medium, suggesting that most of intracellular glutamate derived from glutamine (Figure 2F).

Transcriptomic signature of MELAS 98% mutant cells shows an up-regulation of glutamate and glutamine metabolic pathways. To further gain insights into the transcriptional regulation, gene expression profiling was carried out in 98% mutant cells, compared to control cells. PCA and unsupervised clustering showed a clear-cut difference between 98% mutant load and control cells (Figure 3A). Comparison of the gene expression profile showed a total of 2046 differentially expressed genes with a *p*-value ≤ 0.05 (Fold Change ≥ 1.5) (Supplemental Table 1), with 48% and 52% up-regulated and down-regulated genes in the 98% mutant cells respectively.

Analysis of these genes using the REACTOME pathway database (29) predicted that a total of 955 metabolic pathways were involved in the process, with a *p*-value ≤ 0.05 (Supplemental Table 2). The three main gene clusters involved were: i) the Glutamate and glutamine metabolism (R-HSA-8964539), ii) the Gamma-aminobutyric acid (GABA) synthesis, release, reuptake and degradation; (R-HSA-888590) and iii) the Tricarboxylic Acid Cycle (TCA) cycle (R-HSA-71403) (Table 1). This is in accordance with glutamate and mitochondrial dysregulations revealed by our metabolomic analyses. The expression of a large number of genes involved in the glutamate and GABA pathways were significantly altered (Figure 3B-C). The most upregulated genes were two key genes of the glutamate pathway, namely *GLUD1* and *GAD1*, encoding glutamate dehydrogenase 1 (GDH) and glutamate decarboxylase 1 (GAD1) respectively. GDH converts L-glutamate into alpha-ketoglutarate (αKG), a key step in glutamine anaplerosis whereas GAD1 converts L-glutamate into GABA.

In addition, in 98% mutant cells, several genes involved in the TCA cycle were also upregulated, including those encoding for the Citrate Synthase and Isocitrate Dehydrogenase, as well as most genes encoding for the Succinate Dehydrogenase Complex and genes belonging to the Succinate-CoA Ligase family. It should be noted, however, that *ME3*, encoding the mitochondrial malic enzyme 3 which catalyzes the decarboxylation of malate to pyruvate was found to be down-regulated in mutant cells (Table 1).

Exposure of MELAS cells to KB restores intracellular glutamate level, improves mitochondrial dynamics and respiratory chain activity. We have previously shown that the mitochondrial function of MELAS cells was improved by the switch from glycolysis to fatty acid β-oxidation induced by the KB exposure combining acetoacetate and β-D-hydroxybutyrate *(24)*. We therefore questioned the effect on glutamate levels of exposure to KB for 48 hours on 98% mutant load cells.

The exposure to KB resulted in a 48% reduction of the intracellular glutamate level in the 98% mutant cells, whereas the extracellular glutamate concentration remained unchanged, and no variation of intra- or extracellular glutamate levels was observed in control cells (Figure 4A-B). Similar results on intracellular glutamate level were obtained with the 143B cybrid mutant cells carrying a 98% mutant load of the MELAS mutation, whereas KB exposure significantly increased intracellular glutamate levels in 143B control cells (Supplemental S1 A).

As glutamate has been shown to be toxic to neuronal activity and cell growth (25), we evaluated the protective role of KB, after exposing 98% mutant cells to high glutamate concentrations (30-50μM range). After incubation in standard medium (SM) or KB, cell proliferation of 98% mutant was measured in the presence or absence of glutamate. Cellular growth of 98% mutant cells was fully abolished in the presence of glutamate in SM whereas glutamate did not affect their proliferation in the presence of KB (Figure 4C). We further observed a close inverse correlation between growth rates and intracellular glutamate concentrations (data not shown).

In addition to these effects on cell growth, the exposure of KB also inhibited cell death induced after 15 h incubation with 30 μM of glutamate (Supplemental S1 B).

We next investigated the toxicity of a high intracellular glutamate concentration on the mitochondrial network dynamics. While the mitochondrial network was highly connected in control cells, it was fragmented in the 98% mutant load untreated MELAS cells (Figure 4D1-D2). Interestingly, KB

treatment restored mitochondrial fusion and network elongation in MELAS cells (Figure 4D2). Conversely, control cells exposed to high glutamate concentration presented a mitochondrial swelling and fragmentation, while further addition of KB restored a connected network, demonstrating that KB treatment is protective against glutamate toxicity and restores normal mitochondrial dynamics (Supplementary S1 D1-D2).

Mitochondrial respiration and enzymatic activities are restored by KB exposure in MELAS cells. KB treatment in MELAS cells resulted in a 30% increase of the routine respiration and a 56% increase of maximal respiration capacity compared to untreated 98% mutant cells, while mitochondrial respiration of treated or untreated control cells was unchanged (Figure 5A-B). This was paralleled with a significant 2-fold increase of mitochondrial enzymatic activities of complex I and II, related to citrate synthase, in cells treated with KB for 48 hours, compared to untreated cells (Figure 5C).

The m.3243A>G MELAS variant affects the Glutamate/GABA pathways. Based on our gene expression results, the main enzymes involved in glutamate metabolism pathways, downstream of the transformation of glutamine to glutamate by the glutaminase, were investigated. The first pathway consists in generating αKG from glutamate, by the glutamate dehydrogenase (GDH) (30) (Figure 6A). The second pathway generates succinate by the successive involvement of the glutamate decarboxylase (GAD1), catalyzing the decarboxylation of glutamate to GABA, the 4-Aminobutyrate aminotransferase (ABAT) leading to succinic semialdehyde (SSA), and then the succinate-semi-aldehyde dehydrogenase (SSADH) leading to succinate, the substrate of the complex II (Figure 6A). Importantly, defects in these enzymes are responsible for severe neurometabolic disorders, seizures, intellectual disability and generalized dystonia (30–32).

Gene expression profiling of 98% mutant cells (Figure 3B-C) highlighted the overexpression of *GLUD1*, encoding GDH (Figure 6A and Table 1), prompting us to monitor the conversion of glutamate into αKG by the GDH enzyme. A four-fold increase of GDH activity in 98% mutant cells was observed, paralleling a concomitant overexpression of the protein (Figure 6B-6E1-2), while αKG level remained unchanged in both control and 98% mutant cells (Figure 6C).

Interestingly, GDH enzymatic activity was unchanged by KB exposure, whereas the concentration of αKG, as measured by mass spectrometry, were significantly reduced (71%) in mutant cells exposed to KB (Figures 6C). This suggests that KB stimulates the mitochondrial anaplerotic energy metabolism in mutant cells (26). We also observed that αKG concentration was also increased in KB supplemented control cells (Figure 6C). In addition, GABA levels were reduced in both mutant and control cells exposed to KB by 63% and 48 % respectively (Figure 6D).

We further assessed the protein expression level of GAD1, ABAT and GDH from the glutamate pathway revealing that GAD1 and GDH were significantly two-fold increase in 98% mutant cells. A normal GDH expression level was restored by KB exposure in 98% mutant cells (Figure 6E1-2). Surprisingly, we found in mutant cells that *ABAT* mRNA expression was completely abolished and the protein level was undetectable in western blotting (Figure 6E1-2; Supplementary S2).

Expression level of ABAT protein was unchanged after KB treatment in mutant cells (Figure 6E1-2). In addition, we confirmed the drastic increase of *GAD1* mRNA in the 98% mutant load compared to control cells (Supplementary S2), in line with the *GAD1* overexpression seen in the transcriptomic analysis (Table 1, figure 6E1-2).

Dysfunction of the mitochondrial TCA cycle in MELAS cells is alleviated by KB exposure. The measurements of TCA intermediates by mass spectrometry showed that pyruvate concentration was reduced by 76% in MELAS cells compared to controls, since most of the pyruvate produced during

glycolysis was converted into lactate (Figure 7A-B), as expected in mitochondrial dysfunction (24). Furthermore, citrate concentration was 4 times higher in 98% mutant load than in control cells, representing one of the blockade points of the TCA cycle in 98% mutant cells (Figure 7C), while succinate concentration was reduced by more than half in 98% mutant compared to control cells (Figure 7E). In addition, malate and fumarate concentrations were increased by 319 and 333% respectively, disclosing two additional blocking steps in the TCA cycle related to the reduction of oxidation of different substrates by the NAD+/NADH ratio (Figures 7F-G). The level of αKG remained unchanged between control and 98% mutant cells, suggesting that αKG was converted to glutamate via the GDH bidirectional enzyme, a process further responsible for the glutamate accumulation in mutant cells (Figure 6C -7D).

Interestingly, KB treatment resulted in an 88% reduction of pyruvate concentration (Figure 7A), paralleling a reduction of lactate production in KB-treated 98% mutant cells, compared to untreated cells, suggesting that glycolysis was reduced (Figure 7B). Importantly, KB treatment allowed the TCA cycle to proceed in a more physiological manner, unlocking the various NADH-dependent TCA cycle blockages, as citrate, malate, fumarate and αKG concentrations were significantly lowered by KB treatment (Figure 7C-D-F-G), while succinate concentration was increased (Figure 7E). In KB-treated control cells, a 47% reduction of pyruvate was also observed and a 50% increase of αKG, without any other metabolic change (Figure 7A-D).

The glutamate pathway is altered in brain tissue from a MELAS patient. Mass spectrometry was performed on brain autopsic tissue obtained from a 32-year-old woman who died of MELAS caused by the m.3243A>G variant, and compared to control brains. Higher concentrations of a large number of amino acids (Table 2), including glutamine, glutamate, alanine, proline, arginine, histidine, ornithine, isoleucine, methionine, threonine, valine were found in the MELAS brain, compared to control brains. Most of these amino acids contribute to the glutamate pathway, thus their increase

strongly suggested that glutamate catabolism was also impaired in MELAS brain tissues. Similar to MELAS cells, the concentration of GABA was reduced in the MELAS brain, while immuno-histochemical studies revealed a reduction of GDH, GAD1 and ABAT staining in the frontal lobe, lentiform nucleus, thalamus plus subthalamic nucleus and cerebellum areas from the MELAS brain, compared to 5 control brains (Figure 8A-C).

DISCUSSION

Clinical presentations of mitochondrial disorders caused by pathogenic mtDNA variants are highly heterogeneous due to the peculiarities of the mitochondrial genome (1). Moreover, the development of mitochondrial medicine is also greatly impaired by the lack of biomarkers to monitor the disease outcome and by the absence of efficient therapies targeting mitochondria (1). To tackle these restrictions, in the recent years, substantial progresses were reached using OMICS technologies, providing novel insights into disease mechanisms and opportunities to develop therapeutic routes (27-29).

The m.3243A>G variant is considered as one of the most common mtDNA mutations and the consequences of clinical heterogeneity and mutant load are still not well understood (30). This particular variant is responsible for MELAS syndrome or Maternal Inherited Diabetes and Deafness (MIDD) but also other related clinical disorders (6). Here, we have applied a strategy based on an integrated approach using emerging technologies with the combination of targeted metabolomics with transcriptomics to assess the consequences of m.3243A>G mutation heteroplasmy in a neuronal cell model of MELAS. The main goal was to identify a metabolic signature and relevant pathways, and ultimately monitor the efficacy of nutritional based therapy with the use of ketone bodies.

A multi-OMIC signature of MELAS cells. A specific biochemical signature disclosing key biomarkers of MELAS syndrome was identified, using targeted metabolomics based on high performance liquid chromatography coupled with tandem mass spectrometry and latent variable-based statistical methods. The quantification of 188 metabolites in MELAS neuronal cybrid cells confirmed the significant reduction in arginine and taurine, a result that was already identified in MELAS syndrome, further supporting the therapeutic use of these two key amino acids in MELAS patients with the goal of reducing stroke-like episodes (16, 31, 32).

In addition, metabolomics results evidenced significant increase in L-DOPA, alanine, glutamate and glutamine. L-DOPA accumulation was shown to contribute to mitochondrial dysfunction, in an vitro cellular model of Parkinson's disease (33) whereas increased alanine concentration has been considered as a hallmark of mitochondrial disorders (1). However, the most unexpected result of the metabolomics analysis was the drastic increase of glutamate and glutamine in MELAS cells compared to controls.

*Glutamate is as a key marker of MELAS pathophysiology***.** Glutamate, which dysregulation is frequently encountered in neurological disorders, is a non-essential amino acid crucial for neurotransmission in the central nervous system (34) (35). Glutamate has also a key role to fuel αKG into the mitochondrial TCA (Figure 9A). Defective glutamate uptake was observed in MELAS cybrid cells, associated to the reduction of mitochondrial ATP production (36). Furthermore, extra and intra-cellular glutamate accumulations trigger ROS production and promote apoptosis in neuronal cell models (37, 38).

Our multi-OMIC approach highlighted the metabolic dysregulation of the glutamate pathway, and established tight correlations between intracellular glutamate level, mitochondrial complex I inhibition and the m.3243G>A heteroplasmy level in MELAS cells. These observations were confirmed by transcriptomic data, revealing the glutamate metabolism ontology as one of the most affected in MELAS cells, together with the GABA and TCA cycle pathways. Among these gene clusters, those encoding the key enzymes GAD1 and GDH involved in the glutamate pathway were highly upregulated in mutant cells. This is concordant with what we have previously observed in MELAS 143B cybrid cells, further correlating the transcriptional reprogramming to the heteroplasmy level (39).

Extracellular glutamate concentrations were also significantly elevated in the supernatant of MELAS cybrid neuronal cells, especially those carrying the 70% and 90% mutation loads, while it was also

increased but to a lower extent in the 98% mutant cells. This could possibly be explained by an inhibition of glutamate transport in this latter condition as previously reported (36). The glutamate dysregulation was also confirmed in the MELAS 143B cybrid cell lines, indicating that this dysregulation is not restricted to the neuronal cell type.

Intermediate metabolites of the TCA cycle are increased in MELAS cells. Our metabolomics results revealed the accumulation of TCA cycle intermediates such as citrate, malate and fumarate, evidencing blockades of the TCA cycle in MELAS cells. Importantly, these substrates were related to NADH oxidation, dependent on mitochondrial complex I activity.

These results are fully concordant with those of a recent clinical study performed in

a large cohort of patients harboring the m.3243A>G variant which evidenced the accumulation in plasma of intermediate (29) metabolites of the TCA cycle, linked to NAD+-dependent biochemical reactions. The identification of those metabolites related to NADH redox unbalance is reflecting the disease severity and may be used as biomarkers to follow candidate therapies aiming at reducing NADH reductive stress (40, 41).

In addition, in the context of homoplasmic mtDNA mutations, it has been shown that glutamine, the precursor of glutamate, was used by the TCA cycle, leading to increased synthesis of aspartate (26). Thus, increased amino acid levels, including glutamate, are consistent with a compensatory response to the primary MELAS OXPHOS defect (26, 42).

Mitochondrial dysfunction is alleviated by KB exposure. To monitor if we could reduce the toxic impact of high glutamate concentration, MELAS cells were exposed to a KB treatment, which led to a switch from glycolytic metabolism to mitochondrial fatty acid oxidation. Importantly, MELAS cells exposed to KB unlocked the NADH-dependent TCA cycle blockades, restoring a normal function of the TCA cycle, and significantly increased oxidative metabolism (Figure 9B). Indeed,

analysis of the TCA cycle disclosed the reduction of citrate, malate and fumarate metabolites, all depending on NADH oxidation, thus restoring a close to physiological TCA cycle functioning. These results suggest that a ketogenic diet could provide benefits to treat MELAS disease, as already proposed for other mitochondrial diseases and for drug-resistant epilepsy (20, 22, 23). Further *in vitro* arguments in this way have been recently obtained in our laboratory, showing that KB exposure over a period of 4 weeks alleviates significantly mitochondrial dysfunction in MELAS cells, by improving complex I assembly and activity (21). KB has also been shown to reduce the percentage of deleted mtDNA molecules in cells carrying large-scale heteroplasmic deletions after only 5 days of exposure (43). Other studies have also evidenced that treatment of SH-SY5Y parental cells or complex I deficient cells with decanoid acid, a component of the medium chain triglyceride form of the ketogenic diet, improve mitochondrial functions (44, 45)

In addition, KB exposure reduced the accumulation of glutamate in MELAS mutant cells (Figure 9B), while increasing αKG concentration, suggesting that this latter metabolite is an important marker of anaplerotic energy metabolism (26). αKG plays also a crucial role in the pathophysiology of other mitochondrial disorders and in age-related neurodegenerative diseases, which is most probably related to the reduction of the αKG dehydrogenase complex, as evidenced in age-related neurodegenerative disorders (46). Perturbations of the glutamine/glutamate/αKG metabolic axis were also found in the *Ndufs4* KO mouse model of the Leigh syndrome, while being rescued by mTOR inhibition with rapamycin (47). This latter study also highlighted that αKG is a complex I substrate supporting oxidative phosphorylation (47).

The level of GABA is significantly reduced in MELAS neuronal cells as well as in brain autoptic tissue. In parallel with the accumulation of other amino acids such as glutamate, we observed a significantly reduction of GABA in MELAS neuronal cells without changing the expression level of ABAT, that was confirmed in brain tissue obtained from a MELAS patient. Mitochondrial

dysfunction affects the storage, release or uptake mechanisms of neurotransmitters including glutamate and GABA (48). This is in line with the high prevalence of neuropsychiatric symptoms seen in MELAS patients (49). Uptakes of glutamate and GABA in synaptosomal preparations from mouse brain were also decreased by rotenone in a dose dependent manner (50). Interestingly, it was recently demonstrated that the regulation of GABA availability and signaling was tightly connected through mitochondrial alterations which in turn modulates neuronal communication and social behavior (51). Of note, ABAT variants were also responsible for encephalomyopathies with a neurometabolic disorder of GABA degradation resulting in elevated GABA in brain as well as mtDNA depletion syndrome highlighting ABAT as an enzyme of dual function (52).

As shown in our study, ketogenic diet appears as a promising strategy to modulate mitochondrial function, and eventually mitochondrial biogenesis (21, 53). In this respect, an open label non-randomized clinical trial based on bezafibrate treatment, a molecule known to stimulate mitochondrial biogenesis, was recently evaluated on a limited number of patients carrying the m.3243A>G mutation (54). Results disclosed an alteration of glutamine metabolism with significant increase of several amino acids including, alanine and glutamate, which is thought to be part of a compensatory response to the OXPHOS defect in the context of mtDNA mutation (37, 48).

In conclusion, this work highlights the usefulness of a multi-OMIC strategy and significantly improved our understanding of the contribution of glutamate metabolism to the MELAS pathophysiology, promoting glutamate as a potential biomarker of severity for MELAS syndrome but also revealing the consequences of NADH/ NAD^+ redox imbalance. Metabolic interventions such as ketogenic diet should be considered as a promising therapeutic route to reduce glutamate toxicity, alleviate the blockades of the TCA cycle by reducing NADH reductive stress, due to complex I deficiency in MELAS syndrome.

METHODS

Cell culture. The SH-SY5Y neuronal control cells and mutant cybrid cells carrying the m.3243A>G with 98%, 90% and 70% mutant loads and 143B osteosarcoma cybrid control and mutant cells were cultured in standard DMEM high glucose media (4.5 g/L) or in low glucose (0.5 g/L) (PAN biotech, Aidenbach, Germany), supplemented with 10% fetal bovine serum (PAN biotech), 1% glutamine and 50 µg/mL uridine (Sigma-Aldrich, Saint-Louis, USA) at 37 °C in presence of 5% CO_2 as described elsewhere (16). Control and mutant cybrids in 143B osteosarcoma background were cultured in 2/3 DMEM F-12, 1/3 Amniomax (Gibco) medium supplemented with 10% SVF (PAN biotech), 100 µg/ml sodium pyruvate and 50 µg/ml uridine. Control and mutant cells were exposed to 5 mM of acetoacetate and β-D-hydroxybutyrate (Sigma) in low glucose medium during 48 hours. Control cells were exposed to rotenone (200 nM) a complex I inhibitor during 15 hours.

All cell lines were routinely tested for the absence of mycoplasma contamination. For all experiments, cells were trypsinized, and immediately analyzed for oxygraphic measurements or frozen in liquid nitrogen and stored at -80°C until use.

Deconvolution microscopy. To assess the mitochondrial network (47), cells were incubated during 20 minutes with MitoTracker green FM (Invitrogen™) and 5 min 0.1ug/ml Hoechst 33342 to visualize mitochondria (green) and nucleus (blue). Coverslips were analyzed using an inverted wide-field microscope ECLIPSE Ti-E (Nikon, Tokyo, Japan) equipped with a 100X oil immersion objective (Nikon Plan Apo100x, Tokyo, Japan, N.A. 1.45) and an Andor NEO sCOMS camera con-trolled by Metamorph 7.7 software (Molecular Devices, Sunnyvale, CA). A precision, piezoelectric driver mounted underneath the objective lens allowed faster Z-step movements, keeping the sample immobile while shifting the objective lens. 35-one image planes were acquired along the Z-axis at 0.1mm increments. For mitochondrial network characterization, acquired images were iteratively

deconvolved using Huygens Essential software (Scientific Volume Imaging, Hilversum, The Netherlands), with a maximum iteration scored 50 and a quality threshold at 0.01.

Mitochondrial enzymatic activities. Activities of complexes I, II and SDH (succinate dehydrogenase) of the respiratory chain were measured at 37°C with an UV*mc*^{2} spectrophotometer (SAFAS, Monaco) on mitochondrial enriched fraction. Briefly, cell pellets were resuspended in a volume of 25 µl/million cells of cell buffer (saccharose 250 mM, TRIS 20 mM, EDTA 2 mM, BSA 1mg/mL, pH 7.4). After a freezing-thawing cycle, cells were centrifuged (16000 rpm, 1 min) and resuspended in the same volume of cell buffer. For complex I activity, an additional step of sonication (6 cycles of 5 seconds with a 30 seconds stop) was required. 0.3 million cells were then incubated at 37°C in a reaction medium (KH_2PO_4 100 mM, pH 7.4, KCN 0.5M, Azide 1 mM, BSA 50mg/ml, ubiquinone-1 2.5 mM and DCPIP 5mM). The reaction was started by adding 12mM NADH and the disappearing rate of DCPIP was measured at 600 nm for 2 minutes. The unspecific activity was determined by adding rotenone 2.5 mM at the middle of the kinetic. For complex II activity, 0.5 million cells were added to a reaction buffer (KH_2PO_4 100 mM, pH 7.5, KCN 10mM, EDTA 10 mM, BSA 50mg/ml, rotenone 2.5 mM, antimycin 1 mg/ml, succinate 0.5 M and DCPIP 5 mM) and the reaction was initiated by adding 2.5 mM of ubiquinone-1. The disappearing rate of DCPIP was measured at 600 nm and the background was subtracted by using thenoyltrifluoroacetone 40 mM. For SDH, a volume equivalent to 0.5 million cells was added to the reaction medium (KH_2PO_4 100 mM, pH 7.5 KCN 10mM, succinate 0.5 M and Phenazine methosulfate 20 mM,) and the reaction was initiated by adding 5 mM of DCIP.

Enzymatic activities of the respiratory chain complexes were normalized with respect to citrate synthase activity, measured by adding 0.1 million cells to the following reaction mix (DTNB 1mM, oxaloacetic acid 10 mM, acetyl coA 0.3 mM, triton X100 0.1%) and the appearing rate of CoA-SH was measured at 412 nm.

Mitochondrial respiration measurements. Oxygen consumption was measured in intact cells using an oxygraphic equipment (Oroboros, Innsbruck, Austria). The O_2 consumption was measured in routine respiration, and after complex V inhibition with oligomycin (1mg/ml). The maximal respiration capacity was then measured by the successive additions of increasing doses of FCCP up to maximal respiration rate. The protein concentration was determined using the BCA assay according to the manufacturer recommendations (Pierce, BCA Protein Assay Kit).

Targeted metabolomics analyses of cell homogenates. A targeted, quantitative metabolomic approach using the Biocrates AbsoluteIDQ p180 kit (Biocrates Life sciences AG, Innsbruck, Austria) on an AB Sciex QTRAP 5500 (Life Sciences SCIEX, Villebon sur Yvette, France) mass spectrometer enables the quantification of up to 188 different endogenous molecules, including acylcarnitines, amino acids, biogenic amines, glycerophospholipids, sphingolipids, and sugar as described elsewhere (55). Flow-injection analysis (FIA-MS/MS) was used for quantifying acylcarnitines, glycerophospholipids, sphingolipids and sugar, whereas liquid chromatography (LC) allowed the separation of amino acids and biogenic amines prior to detection with mass spectrometry (LC-MS/MS). Samples were prepared according to the Biocrates Kit User Manual. Briefly, after thawing on ice, metabolites were extracted in a methanol solution using ammonium acetate after drying the filter spot under nitrogen flow and derivatizing with phenylisothiocyanate for the quantification of amino acids and biogenic amines. The extracts were finally diluted with MS running solvent before FIA and LC-MS/MS analysis. After validation of the three levels of quality controls (QCs) used in the kit, the metabolite concentrations were normalized to protein concentrations.

Detection of TCA intermediates using non-targeted metabolomics. In order to complete the targeted signature obtained with Biocrates Absolute IDQ p180 kit, the non-targeted reversed-phase (RP)

metabolomics approach previously validated and published was adapted (56). Cell layers were washed twice with an aqueous solution containing 0.22% NaCl before being quenched with cold MeOH. Cell suspension was then collected in aliquots of one million cells and stored at −80 °C until analysis. Internal quality controls (QCs) were generated by mixing the samples together before the extraction protocol and treated similarly. Krebs cycle intermediates were then extracted adding a mixture of H2O/MeOH. After centrifugation, supernatants were evaporated to dryness and samples were reconstituted with an aqueous solution (2% MeOH) before the UHPLC-HRMS (Ultra High Pressure Liquid Chromatography-High Resolution Mass Spectrometry) analysis in negative mode on a Thermo Scientific Q Exactive mass spectrometer (Thermo Fisher Scientific, Bremen, Germany) coupled to Dionex UltiMate® 3000 UHPLC (Dionex, Sunnyvale, CA, U.S.A.). Ionization conditions, chromatography and MS parameters were identical to those previously described (56-58).

Detection of compounds were performed thanks to a TraceFinder 4.1 processing method based on our in-house commercial database (Mass Spectrometry Metabolite Library of Standards, IROA Technologies, Bolton, MA, U.S.A.) focalized only on TCA intermediates with an identification at level of 1 (59) (m/z ratio lower than 5 ppm, perfect isotopic pattern, RT drift lesser than 5 s, and/or two identical fragments). Several quality parameters were checked: CV (Coefficient of Variation) lower than 30% in QC, a RT drift under 10 sec and a linearity of dilution with an r^2 lower than 0.7. Data were normalized to DNA content of the samples measured by nanoDrop (Nanodrop 1000, Thermo Fisher Scientific, Waltham, MA, U.S.A.).

Metabolite quantification. Glutamate intracellular or extracellular concentrations were quantified following the manufacturer recommendations (Glutamate Assay Kit, Abcam). Amino acid chromatography in brain post mortem tissues was performed using a routine analytical procedure which can accurately detect and quantify 37 amino acids and amino acid-derived molecules by means of an UptiSphere BP2 chromatography column coupled with an API 3000 Triple Quadrupole

Mass Spectrometer (AB Sciex®). Frozen pellets of mutant cells were suspended in 100µL specific lysis buffer (sucrose 250mm, EGTA 0.5mm, HEPES 10mm, Triton 10X and Antiprotease cocktail).

DNA extraction and quantification of mtDNA heteroplasmy. DNA extraction and quantification of the mutant load were performed as described elsewhere (16).

Gene expression profiling. RNA preparation and microarray hybridization: Total RNA was extracted after lysing samples with TRIzol reagent (Life Technologies, Carlsbad, CA, U.S.A.), using the RNeasy Micro kit (Qiagen, Venlo, Netherlands), according to the manufacturer's recommendations. Quantity and quality of the extracted RNA was assessed by microvolume spectrophotometry (Nanodrop 1000, Thermo Fisher Scientific). A Bioanalyzer 2100, with a RNA6000 Nano kit (Agilent Technologies, Santa Clara, CA, U.S.A.) was used to assess RNA quality. A RNA integrity number of 7·00 or more was achieved for all samples. Biotinylated, amplified cRNA was generated using the Illumina Total Prep RNA Amplification kit (Ambion, Life Technologies, Carlsbad, CA, U.S.A.), according to the manufacturer's recommendations. cRNA was hybridized on Illumina HumanHT-12 v4 Expression BeadChips, stained and detected with the iScan system, according to the manufacturer's protocol (Illumina, San Diego, CA, U.S.A.). GenomeStudio 2011 (version 1) and its Expression Analysis Module (version 1.9.0) were used for signal extraction and quantile normalization (Illumina). Gene expression profile datasets are available from the following database: GEO accession number GSE165953.

Quality assessments, normalization and statistical analysis of gene expression. Data were analyzed using R version 3.6.3 (60) and Rstudio version 1.3.959. Raw data matrixes were extracted from .idat files using Illumina package (61). For the normalization step, we applied a quantile normalization using Limma with a log2 transformation to obtain normalized data matrix (62, 63). As quality

control, unsupervised analysis was assessed using hierarchical clustering (Pearson's dissimilarity and complete linkage) and Principal Component Analysis (PCA). No technical bias or outlier sample had to be taken into account in the downstream analysis. To find differentially expressed genes between MELAS and control cells we applied a t-test on gene variables. Fold-changes were computing with delog values. Functional analyses were made through the use of MSigDB genesets database (64) using binomial enrichment tests. Expression data are available through the NCBI Gene Expression Omnibus (GEO; Accession number: GSE165953 on GEO NCBI site.

Quantitative PCR. Total RNA was purified using a RNeasy Mini Kit (Qiagen) according to the manufacturer's protocol. 2 µg of RNA were reverse transcribed and qRT-PCR was performed in triplicates (Applied Biosystems). Each reaction (final volume 10µl) contained 100 ng of cDNA, 5µl of Power SYBR-Green PCR Master Mix (Applied Biosystems) and 0.5µM of each forward and reverse primers. Two sets of primers were designed to measure the mRNA expression level of GAD67, ABAT and *GAPDH and actin* was used as loading control (primer sequences are available on request).

Western Blot analysis. Frozen pellets of cells were resuspended in 1X protease inhibitor cocktail (Complete Protease Inhibitor Cocktail Tablets, Roche Applied Science, Bale Switzerland) and 1X RIPA (Radioimmunoprecipitation assay) buffer. A volume corresponding to 50 µg protein for GDH and GAD or 90µg for ABAT was added to a Laemmli buffer (277.8 mM Tris-HCL pH 6.8, 44.4% (v/v) glycerol, 4.4% LDS, 0.02% bromophenol blue, Bio Rad) supplemented with β-mercaptoethanol (10%), boiled for 5 minutes and loaded on 12.5% Tris-SDS-acrylamide gel. Proteins were separated by electrophoresis and transferred onto PVDF membranes (BioRad). Membranes were blocked with TBS 1X (NaCl 0.8%, KCl 0.02%, Tris 0.3%, pH 7.4), Tween 0.01%, 5% non-fat milk for 2 hours and incubated with primary antibodies GAD1, GDH, ABAT, (Abcam) overnight at 4°C. Incubation

with a secondary antibody (anti-mouse or anti-rabbit, GE Healthcare) was performed for two hours at room temperature. The different proteins were visualized by enhanced chemiluminescence using appropriate kit on a LI-COR Odyssey apparatus. Proteins are quantified using ImageStudio software (Li- COR Odyssey). Tubulin or Actin antibodies (Abcam) were used as loading controls.

Immunocytochemistry. 5 mm-thick slices were cut from formalin-fixed, paraffin-embedded brain biopsy blocks using a Leica RM125 microtome. Imunohistochemistry was carried out using an automated slide immunostainer (Leica Bond Max). Briefly, slices were deparaffinized prior to antigen exposure pretreatment at 100°C for 20 min in epitope retrieval solution (EDTA-buffer pH8.8). Incubation for 10 minutes with a rabbit monoclonal primary antibody targeting GAD1, ABAT or GDH was followed by an immunoperoxidase-based detection and a hematoxylin counterstain. Staining was examined microscopically and scored semi-quantitatively as follows: 0 = absent, + = mild, ++ = moderate and +++ = strong.

Statistical analysis. Data are presented as means +/- SEM of at least 4 independent experiments. Differences between groups are evaluated by Mann-Whitney statistical test using GraphPad Prism software (GraphPad software, San Diego, USA), asterisk and the sharp sign (* and #) indicates *p-value* <0.05, (** and ##) *p-value* <0.001, (***) *p-value* <0.0001.

Study approval. Patient samples were obtained after informed consent (Institutional Review Board Committee of the University Hospital of Angers, Authorization number: AC-2012-1507). Post mortem brain tissue samples of a MELAS individual, a woman who died at 32 years of age, and age-gender matched control brain samples were collected and frozen immediately after death.

FIGURES AND FIGURE LEGENDS

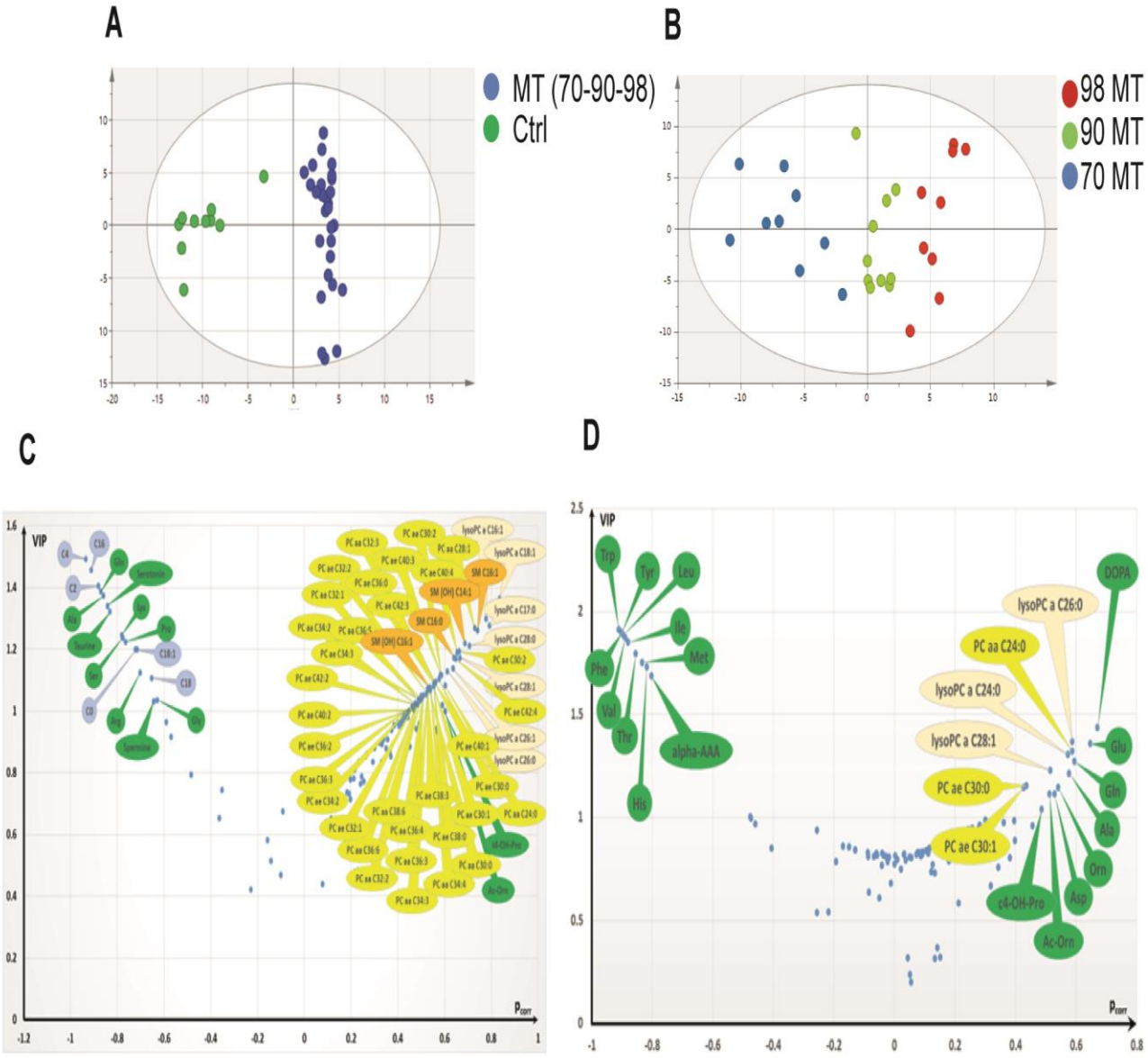

Figure 1. Metabolomic analysis between MELAS and control cells

(A) Unsupervised PCA analysis of metabolomics data from parental Ctrl cells (n=10, green dots) and mutant (MT) cells carrying different m.3243A>G mutant loads (n=30, blue dots). The first two principal components (PC1 and PC2) explain more than 75% of the total variance. The first component (PC1) clearly separates Ctrl *vs* MT cells. The supervised model has good predictive discriminant properties (q2cumulated = 0.57) and explains up to 68% of the variance of the y vector.

(B) OPLS model scatter plot of MELAS cells carrying different MT loads. MT cybrids are separated according to the mutant load: 70% (blue circles), 90% (green circles) and 98% (red circles), along the predictive latent variable (LVp).

(C) Supervised OPLS-DA models for MT cells with 70%, 90% to 98% mutant loads *vs* parental cells. Only the most discriminating metabolites with high VIP values (>1) and coefficient values (≥ 0.02 or ≤ -0.02) have been labelled. Negative coefficients (left) indicate diminished metabolite concentrations in MT cells versus parental cells, whereas positive coefficients (right) indicate increased metabolite concentrations.

Amino acids and biogenic amines are represented as green bubbles; phosphatidylcholines (PC) as yellow bubbles and lysophosphatidylcholines (lysoPC) as pink bubbles. In PC, "aa" indicates that both moieties at the sn-1 and sn-2 position are fatty acids and bound to the glycerol backbone via ester bonds, whilst "ae" denotes that one of the moieties, either in the sn-1 or at sn-2 position is a fatty alcohol and bound via an ether bond. For lysoPCs and PCs, the total number of carbon atoms and double bonds present in lipid fatty acid chain(s) are denoted as "C x:y", where x is the total carbon number (of both chains for PCs) and y is the total number of double bonds. Ala: Alanine; alpha-AAA: α-Aminoadipic acid; Ac-Orn: Acetyl-ornithine; Asp: Aspartate; c4-OH-Pro: cis-4-Hydroxyproline; DOPA: 3,4-Dihydroxyphenylalanine; Gln: Glutamine; Glu: Glutamate; His: Histidine; Ile: Isoleucine; Leu: Leucine; Met: Methionine; Orn: Ornithine; Phe: Phenylalanine; Thr: Threonine; Trp: Tryptophane; Tyr: Tyrosine; Val: Valine.

The metabolic signature is characterized by lower levels of 6 acylcarnitines (C0, C2, C4, C16, C18, C18:1) (blue bubbles), 10 amino acids and amine biogenes (green bubbles) and higher levels of several PC (yellow bubbles) and sphingomyelins (orange bubbles).

Ala: Alanine, Gln: Glutamine, Ser: Serine, Lys: Lysine, Pro: Proline, Gly: Glycine, Arg: Arginine, Taurine, Serotonin and Spermine.

(D) Loadings (p_{corr}) *vs* VIP or "volcano" plot for the OPLS-DA model obtained from the metabolomics analysis of MELAS cells with the 70%, 90%, 98% mutant loads. Only the most discriminating metabolites with high variable importance in the projection (VIP) values (>1) and coefficient values (≥ 0.02 or ≤ -0.02) have been labelled. Negative coefficients (left) indicate lower metabolite concentrations in 70% and 90% MT cells, whereas positive coefficients (right) indicate metabolites with higher concentrations in 98% MT cells.

Amino acids and biogenic amines are represented as green bubbles; phosphatidylcholines (PC) as yellow bubbles and lysophosphatidylcholines (lysoPC) as pink bubbles.

Ala: Alanine; alpha-AAA: α-Aminoadipic acid; Ac-Orn: Acetyl-ornithine; Asp: Aspartate; c4-OH-Pro: cis-4-Hydroxyproline; DOPA: 3,4-Dihydroxyphenylalanine; Gln: Glutamine; Glu: Glutamate; His: Histidine; Ile: Isoleucine; Leu: Leucine; Met: Methionine; Orn: Ornithine; Phe: Phenylalanine; Thr: Threonine; Trp: Tryptophan; Tyr: Tyrosine; Val: Valine.

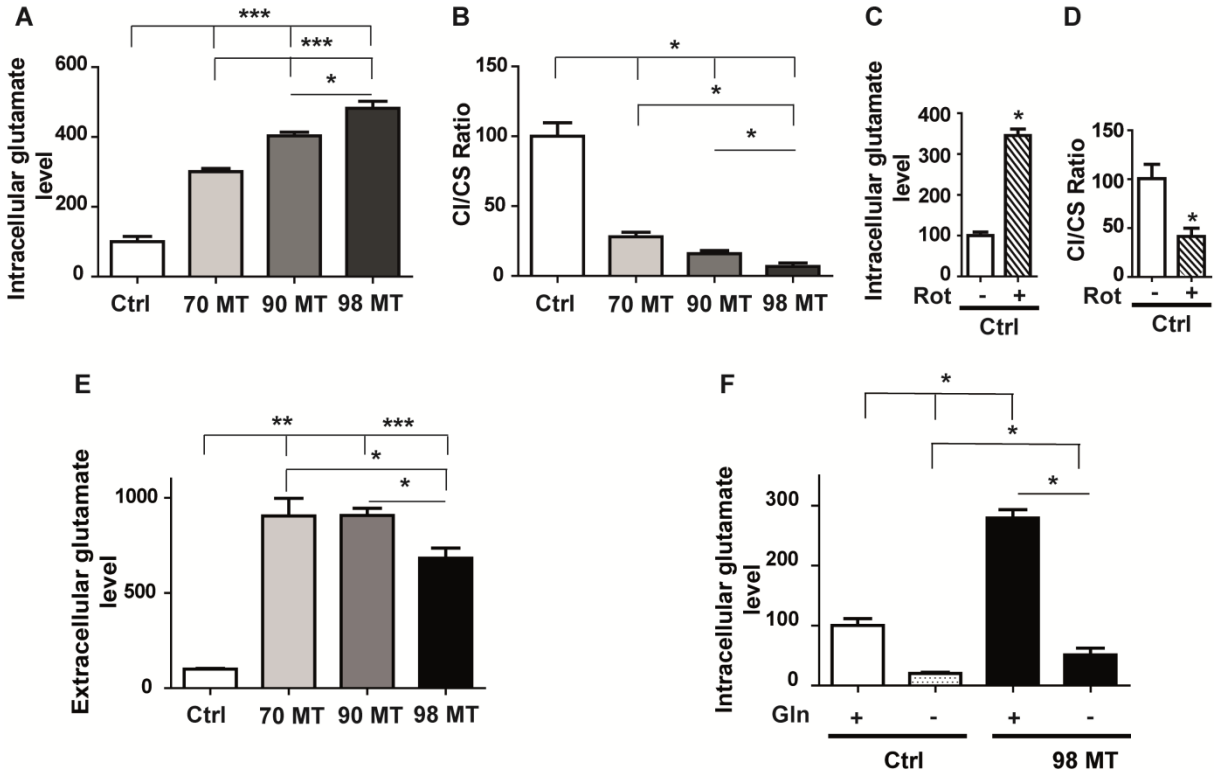

Figure 2. Glutamate concentration is correlated with complex I deficiency in MELAS cells.

(**A**) Intracellular levels of glutamate in control (Ctrl) and mutant (MT) cells (70%, 90% and 98%). (**B**) Biochemical assessment of mitochondrial complex I activity in Ctrl and MT cells (70%, 90% and 98%). **(C)** Intracellular level of glutamate in Ctrl cells treated for 15 hours with rotenone (200nM) or vehicle. **(D)** Biochemical assessment of mitochondrial complex I activity in Ctrl cells treated for 15 hours with rotenone or vehicle. (**E**) Extracellular glutamate levels. Ctrl: control cells and MT cells carrying different mutant loads (70%, 90% and 98%). **(F)** Intracellular glutamate levels in Ctrl and 98% MT cells with (+) or without (-) addition of glutamine. Results are presented as means ± SEM relative to Ctrl cells, of at least 4 independent experiments. Statistical differences are indicated with an asterisk between MT and Ctrl cells (*p<0.05; ** p<0.01; *** p<0.001).

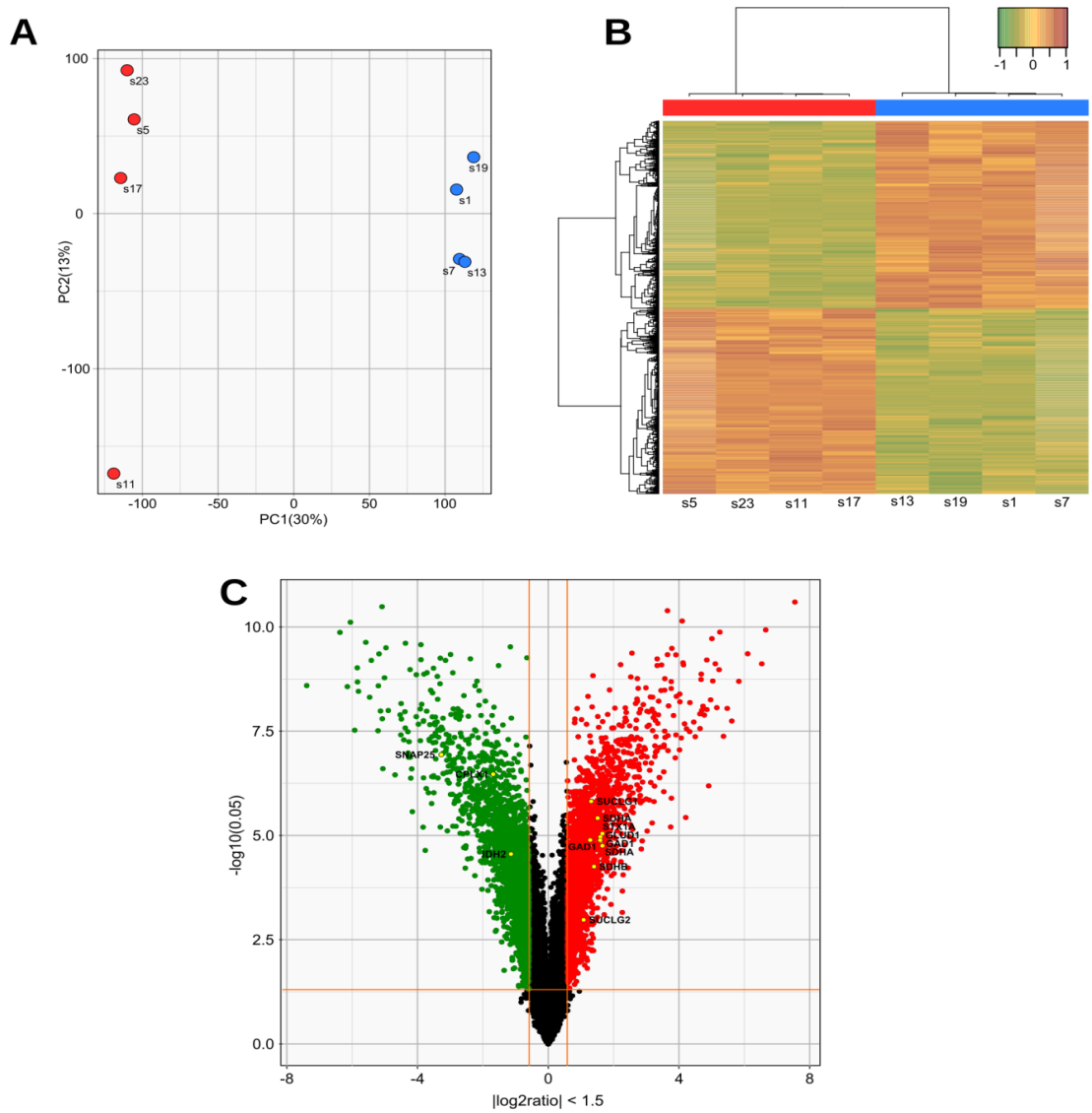

Figure 3. Gene expression profiling of mutant cells.

(A) Principal component analysis (PCA) and unsupervised clustering of MT *vs* Ctrl cells.

(B) Heatmap diagram of a two-way hierarchical clustering analysis of the 4943 probes, showing different expression levels with a p-value ≤ 0.05 and abs(FC) ≥1.5. Red and green colors represent an expression level above or lower the mean, respectively. X-axis represents samples with, from the left to the right, control cells compared to 98% MT cells (n=4) and Y-axis represents Illumina probes. **(C)** Volcano plot representation of the differentially expressed genes in a pairwise comparison of control *vs* 98% MT cells. The significant cut-off was set to a p-value ≤0.05 and abs(FC) ≥1.5. Differentially expressed genes annotated as glutamate-glutamine metabolism, GABA and TCA cycle from the REACTOME pathway Database (see Table 1) are labeled with their corresponding gene symbols.

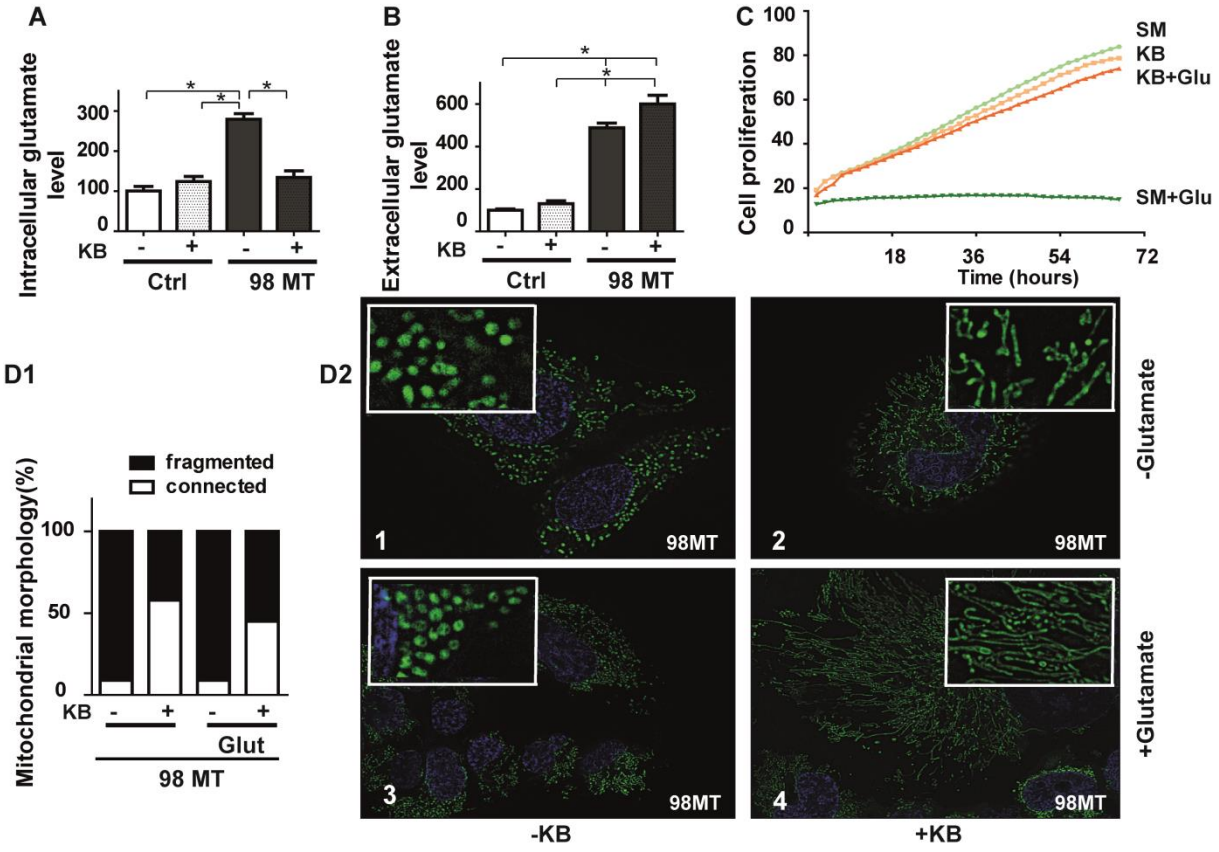

Figure 4. Treatment with ketone bodies restores a normal intracellular glutamate concentration and improves mitochondrial network in MELAS cells.

(**A**) Intracellular and **(B)** extracellular glutamate levels in Ctrl and 98% MT cells treated for 48 hours with (+) or without (-) ketone bodies (KB). Results are from at least four independent experiments, expressed as means ± SEM relative to Ctrl cells. (*p<0.05). (**C**) Cell growth of 98% MT cells cultured in standard medium (SM, light green curve), or exposed to ketone bodies alone (KB, orange curve), or with 50µM glutamate (Glu) and ketone bodies (KB+Glu, red curve) or standard medium (SM+Glu, green curve). (**D1**) Mitochondrial morphology, and percentages of fragmented (black) or connected mitochondria (white) in 98% MT cells with (+) or without (-) KB, and with or without glutamate (30µM). (**D2**) Representative images showing the MitoTracker (green fluorescence) and Hoechst (blue fluorescence) staining of 98% MT cells, incubated for 24h in D2-1: standard medium, D2-2: with ketone bodies (KB), D2-3: with glutamate (Glu) and D2-4: with Glu and KB.

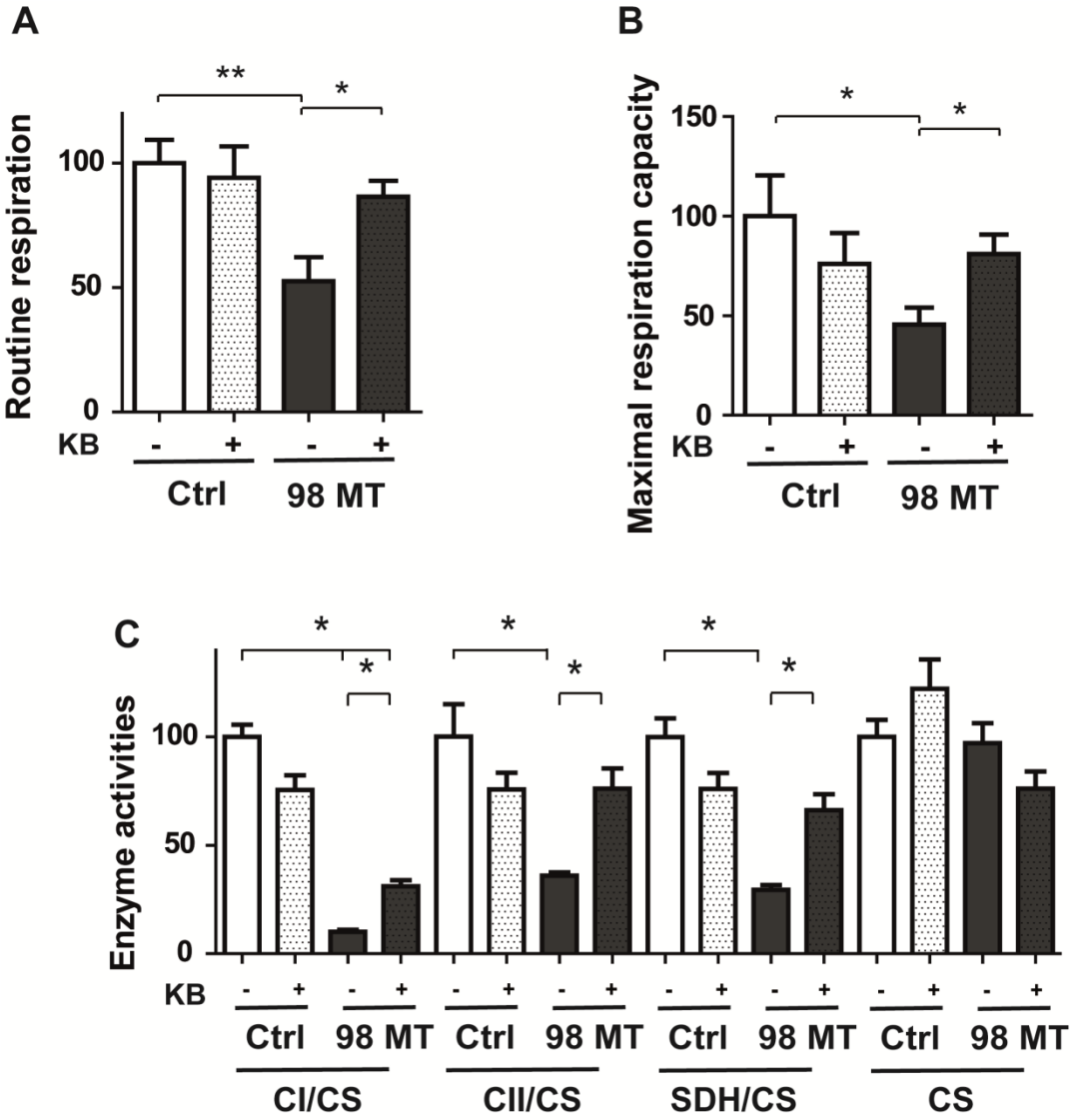

Figure 5. Treatment with ketone bodies improves mitochondrial respiration and enzyme activities in MELAS cells.

(**A**) Oxygraphic measurements of routine (**B**) and maximal respiration capacity in Ctrl and 98% MT cells, treated with or without ketone bodies (KB) for 48h. (**C**) Enzymatic activities of mitochondrial complex I, II, and SDH, relatively to citrate synthase (CS) in control and 98% MT cells, treated for 48h with or without KB. Results are presented as means ± SEM, relative to Ctrl cells, of at least 4 independent experiments. Statistical differences between 98% MT and Ctrl cells are indicated with an asterisk (*$p<0.05$; ** $p<0.01$).

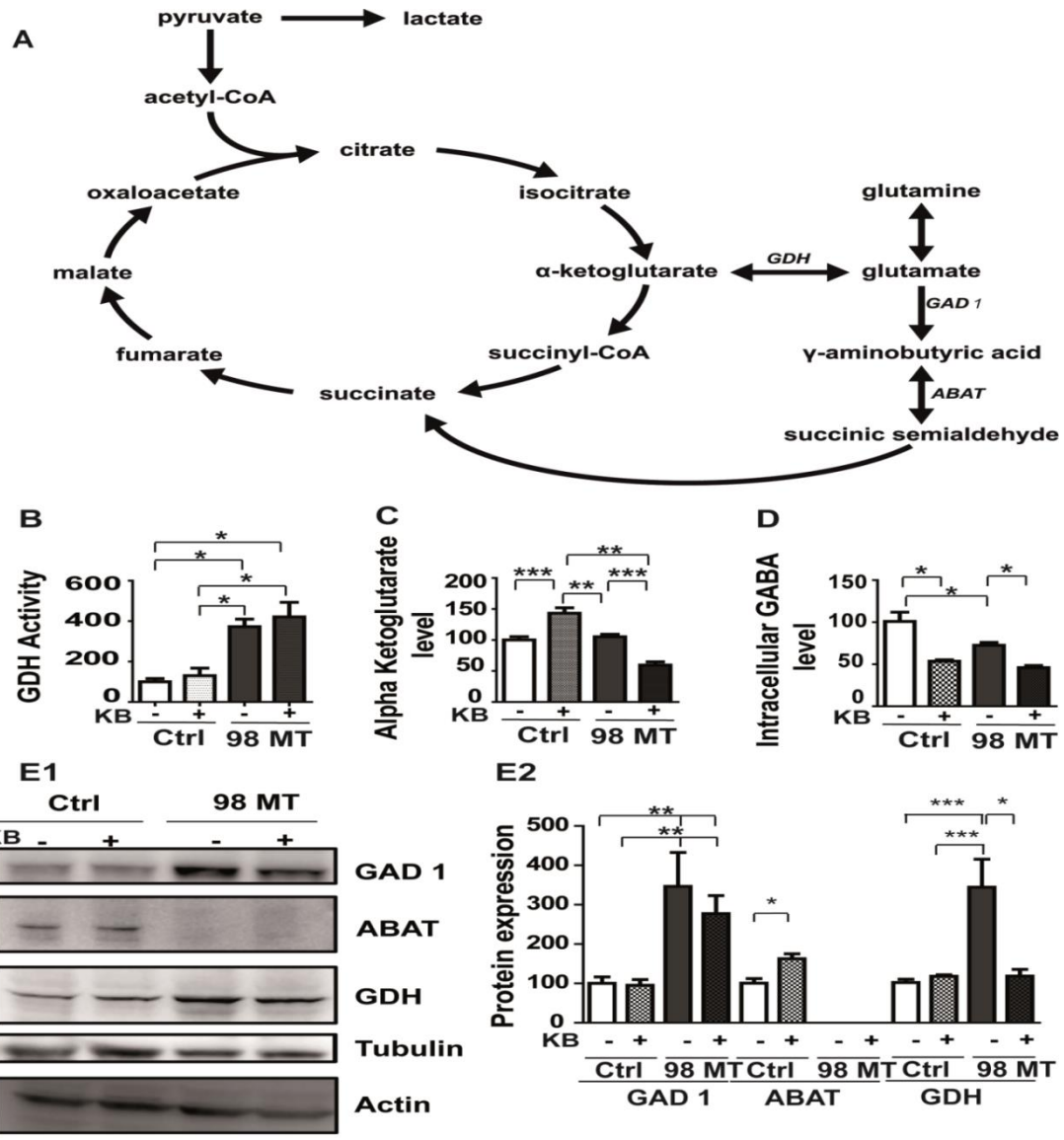

Figure 6. The Glutamate and GABA metabolic pathways are altered in MELAS cells.

(**A**) Graphical representation of the glutamate pathway and TCA cycle. GAD1 (glutamate decarboxylase), ABAT (4 aminobutyrate transaminase) and GDH (glutamate dehydrogenase). (**B**) Measurement of GDH activity, (**C**) intracellular levels of alpha ketoglutarate concentrations and (**D**) intracellular levels of GABA in Ctrl and 98% MT cells, exposed for 48h with (+) or without (-) ketone bodies (KB). (**E1**) Western blots showing GAD1, ABAT and GDH expression profiles in Ctrl and 98% MT cells, treated for 48h with (+) or without (-) KB. (**E2**) Quantification of GAD1, ABAT and GDH relative expression related to tubulin and actin, in Ctrl and 98% MT cells treated with (+) or without (-) KB. Results are presented as means ± SEM, relative to Ctrl cells of at least 4 independent experiments. Statistical differences are indicated with an asterisk between 98% MT and Ctrl cells (*p<0.05; ** p<0.01; *** p<0.001).

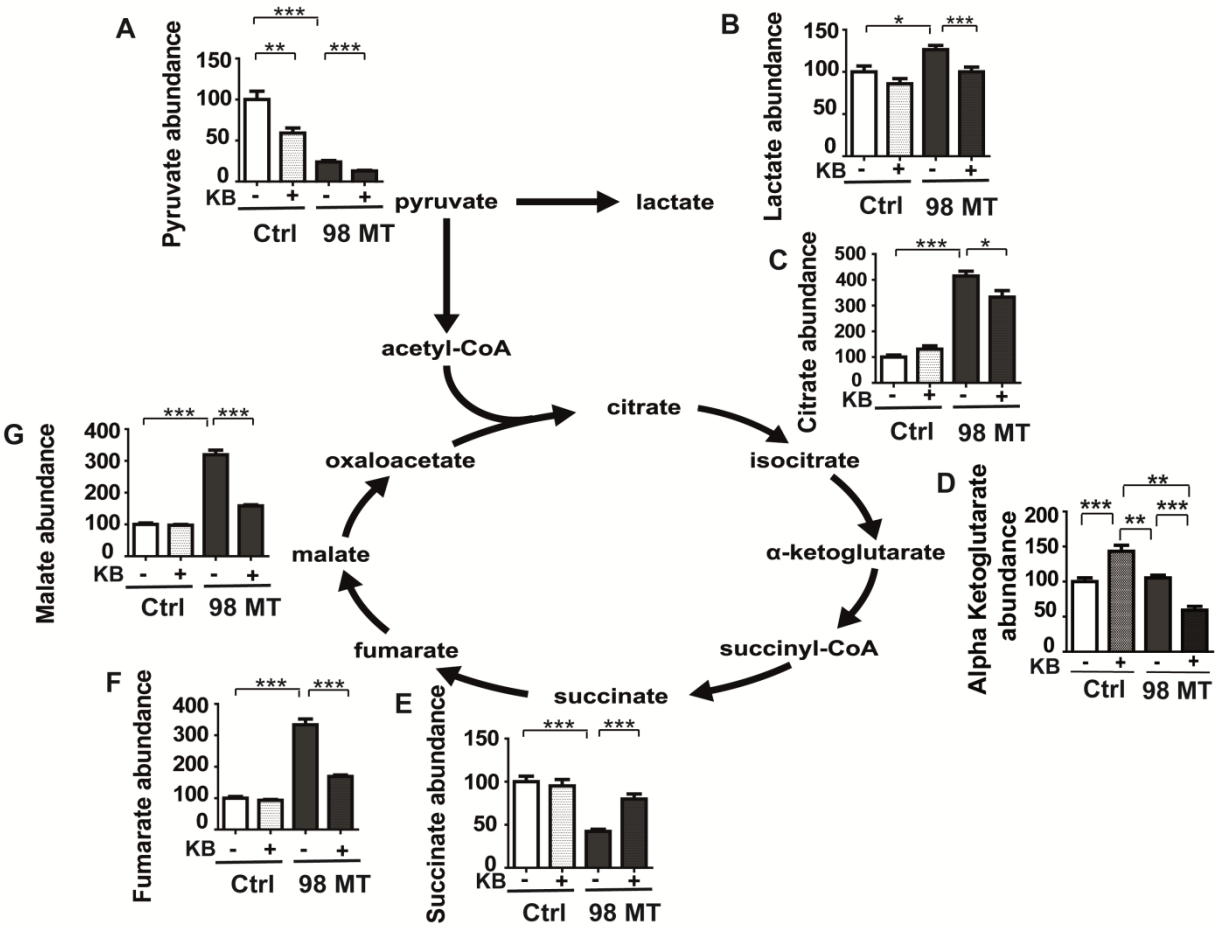

Figure 7. TCA cycle dysfunction in MELAS cells is alleviated by ketone bodies

(**A**) Pyruvate, (**B**) lactate, (**C**) citrate, (**D**) alpha-ketoglutarate, (**E**) succinate, (**F**) fumarate and (**G**) malate levels in Ctrl and 98% MT cells for 48h treated with (+, doted line) or without (-, color bar) ketone bodies (KB). Results are presented as means ± SEM relative to Ctrl cells of at least 4 independent experiments. Statistical differences are indicated with an asterisk between 98% MT and Ctrl cells (*p<0.05; ** p<0.01; *** p<0.001).

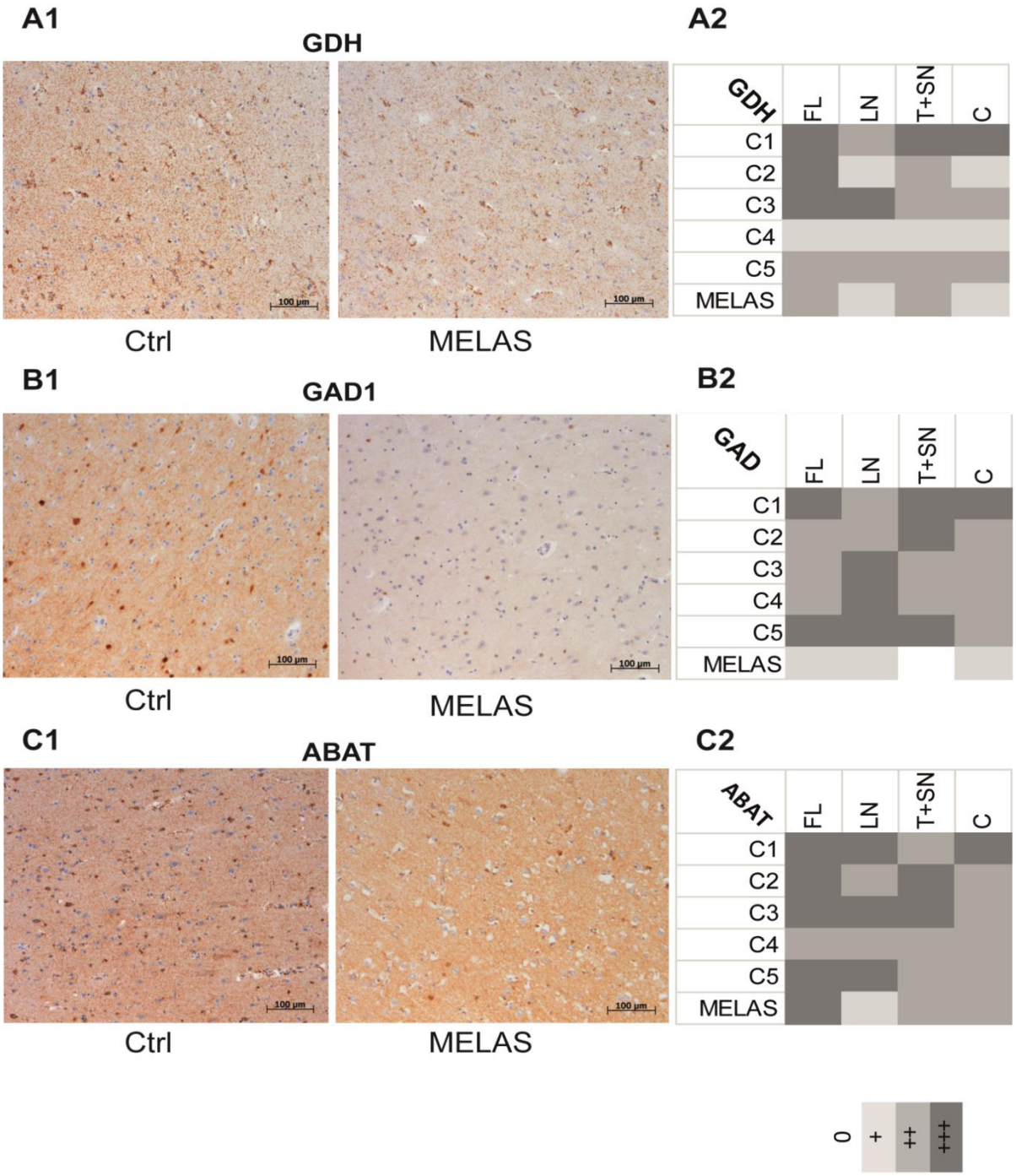

Figure 8. The glutamate pathway is altered in the brain tissues from a MELAS patient. Immuno-histochemical analyses of paraffin-embedded human frontal brain tissues labeled with GDH (**A1-A2**), GAD1 (**B1-B2**) and ABAT (**C1-C2**) antibodies, from Ctrl individuals (left panel) and a MELAS patient (right panel). Immuno-histochemical staining intensities of GDH (**A2**), GAD1 (**B2**) and ABAT (**C2**) were examined microscopically and scored semi-quantitatively by 2 independent analyses on 5 Ctrl individuals and one MELAS patient, as follow: 0 = absent, + = mild, ++ = moderate and +++ = intense. FL: frontal lobe; LN: lentiform nucleus; T+SN: thalamus + subthalamic nucleus, C: cerebellum.

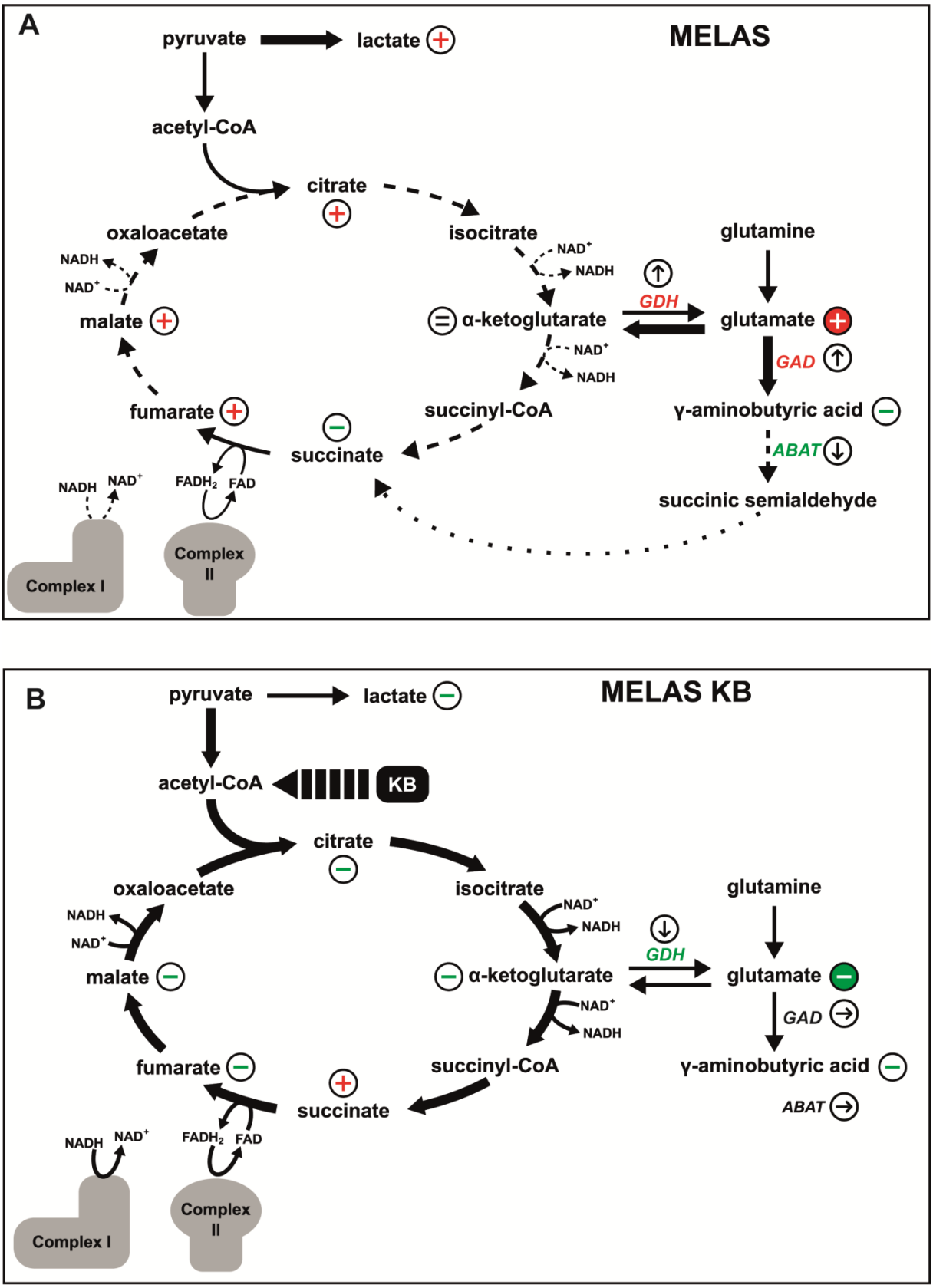

Figure 9. Graphical representation of metabolic pathways of MELAS cells (**A**) untreated (**B**) or treated with ketone bodies (KB). +: metabolite increase. –: metabolite reduction, = metabolite unchanged. ↑: increased gene expression ↓: decreased gene expression.

Pathway ID	Pathway Description	Up-regulated genes	Down-regulated genes	Unchanged genes
R-HSA-8964539	Glutamate and glutamine metabolism	***ALDH18A1, GLUD1, GOT2, KYAT1, OAT, RIMKLB***	***PYCR1***	*GLS, GLS2, GLUD2, GLUL, PYCR2, PYCR3, RIMKLA*
R-HSA-888590	GABA synthesis, release, reuptake and degradation	***GAD1, HSPA8, SLC6A1, STX1A, VAMP2***	***ALDH5A1, CPLX1, SNAP25, SYT1***	*ABAT, DNAJC5, GAD2 RAB3A, RIMS1,SLC32A1 SLC6A11, SLC6A12, SLC6A13, STXBP1*
R-HSA-71403	TCA cycle	***CS, DLST, IDH3A, IDH3B, IDH3G, OGDH, SDHA, SDHB SDHD, SUCLA2, SUCLG1 SUCLG2***	***FAHD1, IDH2, ME3, NNT, SDHC***	*ACO2, DLD, FH, MDH2, ME2*

Table 1. Functional classification analysis of repressed or overexpressed genes in MELAS cells according to the REACTOME pathway database. The three key clusters (glutamate, GABA, and TCA cycle) from the reactome are shown. Genes belonging to "Glutamate and glutamine metabolism", "GABA synthesis, release, reuptake and degradation" and "TCA cycle" were classified in three groups. The up-regulated genes with a pvalue ≤ 0.05 and FC ≥1.3, down-regulated genes with a pvalue ≤0.05 and FC≤-1.3 and unchanged gene expression if the pvalue >0.05 and/or abs (FC) <1.3. Up-regulated and down regulated genes from these pathways with a fold change over 1.5 are indicated in bold.

Amino acids	Ctrls	MELAS patient
Glutamate	**239**+/-15.5	**417**
Glutamine	**246.5**+/-0.7	**356**
Proline	**29.7**+/-0.42	**60.1**
Arginine	**21.8**+/-0.28	**52.9**
Histidine	**16.35**+/-2.19	**25.4**
Ornithine	**10.75**+/-0.07	**9.9**
Isoleucine	**16.1**+/-1.7	**40.5**
Methionine	**9.64**+/-1.64	**25.5**
Threonine	**25.15**+/-1.62	**44**
Valine	**25.9**+/-2.54	**62.3**
Alanine	**99.25**+/-3.9	**168**
Aspartate	**133**+/-9.89	**108**
GABA	**93.25**+/-7.2	**66.9**

Table 2. Mass spectrometry quantification of amino acids in autopsic brain tissues from *Ctrl*s and a MELAS patient. Controls: Ctrls; Ctrl values (n= 2) are expressed as means ± SEM.

AUTHOR CONTRIBUTIONS

Conceptualization: S.B., A.C., V.P.; Formal Analysis and Data curation: S.B., D.G., C.B., F.D., J.C.B., V.D.D., N.G., G.G., R.B., S.K., C.B., T.A., D.S., A.I., A.R., V.P.; Investigation and Resources: M.B., C.V., M.B., D.B., G.S., P.R., F.L., G.L., A.C., V.P. Writing – original draft V.P., S.B.; A.C., G.L.; D.B. Writing – review & editing: input from all authors, who approved the final version of the manuscript.

ACKNOWLEDGMENTS

This work was supported by grants from: "Association Française contre les Myopathies" Mitoscreen 17122, Fondation pour la Recherche Médicale" DPM20121125554, AMMi "Association contre les Maladies Mitochondriales" and supports from the University and the University Hospital of Angers, CNRS and INSERM.

REFERENCES

1. Wallace DC, Fan W, and Procaccio V. Mitochondrial energetics and therapeutics. *Annu Rev Pathol.* 2010;5(297-348.
2. Wallace DC. A mitochondrial paradigm of metabolic and degenerative diseases, aging, and cancer: a dawn for evolutionary medicine. *Annu Rev Genet.* 2005;39(359-407.
3. Wallace DC. Why do we still have a maternally inherited mitochondrial DNA? Insights from evolutionary medicine. *Annual Review of Biochemistry.* 2007;76(781-821.
4. Goto Y, Nonaka I, and Horai S. A mutation in the tRNA(Leu)(UUR) gene associated with the MELAS subgroup of mitochondrial encephalomyopathies. *Nature.* 1990;348(6302):651-3.
5. Hirano M, Ricci E, Koenigsberger MR, Defendini R, Pavlakis SG, DeVivo DC, DiMauro S, and Rowland LP. Melas: an original case and clinical criteria for diagnosis. *Neuromuscul Disord.* 1992;2(2):125-35.
6. El-Hattab AW, Adesina AM, Jones J, and Scaglia F. MELAS syndrome: Clinical manifestations, pathogenesis, and treatment options. *Mol Genet Metab.* 2015;116(1-2):4-12.
7. Chomyn A, Martinuzzi A, Yoneda M, Daga A, Hurko O, Johns D, Lai ST, Nonaka I, Angelini C, and Attardi G. MELAS mutation in mtDNA binding site for transcription termination factor causes defects in protein synthesis and in respiration but no change in levels of upstream and downstream mature transcripts. *Proc Natl Acad Sci U S A.* 1992;89(10):4221-5.
8. Kirino Y, Yasukawa T, Ohta S, Akira S, Ishihara K, Watanabe K, and Suzuki T. Codon-specific translational defect caused by a wobble modification deficiency in mutant tRNA from a human mitochondrial disease. *Proc Natl Acad Sci U S A.* 2004;101(42):15070-5.
9. Uusimaa J, Moilanen JS, Vainionpaa L, Tapanainen P, Lindholm P, Nuutinen M, Lopponen T, Maki-Torkko E, Rantala H, and Majamaa K. Prevalence, segregation, and phenotype of the mitochondrial DNA 3243A>G mutation in children. *Ann Neurol.* 2007;62(3):278-87.
10. Finsterer J. Genetic, pathogenetic, and phenotypic implications of the mitochondrial A3243G tRNALeu(UUR) mutation. *Acta Neurol Scand.* 2007;116(1):1-14.
11. Koopman WJ, Willems PH, and Smeitink JA. Monogenic mitochondrial disorders. *N Engl J Med.* 2012;366(12):1132-41.
12. Sproule DM, and Kaufmann P. Mitochondrial encephalopathy, lactic acidosis, and strokelike episodes: basic concepts, clinical phenotype, and therapeutic management of MELAS syndrome. *Ann N Y Acad Sci.* 2008;1142(133-58.
13. Dunbar DR, Moonie PA, Zeviani M, and Holt IJ. Complex I deficiency is associated with 3243G:C mitochondrial DNA in osteosarcoma cell cybrids. *Hum Mol Genet.* 1996;5(1):123-29.
14. Hamalainen RH, Manninen T, Koivumaki H, Kislin M, Otonkoski T, and Suomalainen A. Tissue- and cell-type-specific manifestations of heteroplasmic mtDNA 3243A>G mutation in human induced pluripotent stem cell-derived disease model. *Proc Natl Acad Sci U S A.* 2013;110(38):E3622-30.
15. Majamaa K, Rusanen H, Remes A, and Hassinen IE. Metabolic interventions against complex I deficiency in MELAS syndrome. *Mol Cell Biochem.* 1997;174(1-2):291-6.
16. Desquiret-Dumas V, Gueguen N, Barth M, Chevrollier A, Hancock S, Wallace DC, Amati-Bonneau P, Henrion D, Bonneau D, Reynier P, et al. Metabolically induced heteroplasmy shifting and l-arginine treatment reduce the energetic defect in a neuronal-like model of MELAS. *Biochim Biophys Acta.* 2012;1822(6):1019-29.
17. Geffroy G, Benyahia R, Frey S, Desquiret-Dumas V, Gueguen N, Bris C, Belal S, Inisan A, Renaud A, Chevrollier A, et al. The accumulation of assembly intermediates of the mitochondrial complex I matrix arm is reduced by limiting glucose uptake in a neuronal-like model of MELAS syndrome. *Biochim Biophys Acta Mol Basis Dis.* 2018;1864(5 Pt A):1596-608.

18. Shanske S, Coku J, Lu J, Ganesh J, Krishna S, Tanji K, Bonilla E, Naini AB, Hirano M, and DiMauro S. The G13513A mutation in the ND5 gene of mitochondrial DNA as a common cause of MELAS or Leigh syndrome: evidence from 12 cases. *Arch Neurol.* 2008;65(3):368-72.
19. Koga Y, Povalko N, Nishioka J, Katayama K, Yatsuga S, and Matsuishi T. Molecular pathology of MELAS and L-arginine effects. *Biochim Biophys Acta.* 2012;1820(5):608-14.
20. Bough KJ, and Rho JM. Anticonvulsant mechanisms of the ketogenic diet. *Epilepsia.* 2007;48(1):43-58.
21. Frey S, Geffroy G, Desquiret-Dumas V, Gueguen N, Bris C, Belal S, Amati-Bonneau P, Chevrollier A, Barth M, Henrion D, et al. The addition of ketone bodies alleviates mitochondrial dysfunction by restoring complex I assembly in a MELAS cellular model. *Biochim Biophys Acta Mol Basis Dis.* 2017;1863(1):284-91.
22. Kang HC, Lee YM, and Kim HD. Mitochondrial disease and epilepsy. *Brain Dev.* 2013;35(8):757-61.
23. Steriade C, Andrade DM, Faghfoury H, Tarnopolsky MA, and Tai P. Mitochondrial encephalopathy with lactic acidosis and stroke-like episodes (MELAS) may respond to adjunctive ketogenic diet. *Pediatr Neurol.* 2014;50(5):498-502.
24. Sasarman F, Antonicka H, and Shoubridge EA. The A3243G tRNALeu(UUR) MELAS mutation causes amino acid misincorporation and a combined respiratory chain assembly defect partially suppressed by overexpression of EFTu and EFG2. *Hum Mol Genet.* 2008;17(23):3697-707.
25. Plotegher N, Filadi R, Pizzo P, and Duchen MR. Excitotoxicity Revisited: Mitochondria on the Verge of a Nervous Breakdown. *Trends Neurosci.* 2021.
26. Chen Q, Kirk K, Shurubor YI, Zhao D, Arreguin AJ, Shahi I, Valsecchi F, Primiano G, Calder EL, Carelli V, et al. Rewiring of Glutamine Metabolism Is a Bioenergetic Adaptation of Human Cells with Mitochondrial DNA Mutations. *Cell Metab.* 2018;27(5):1007-25 e5.
27. Khan S, Ince-Dunn G, Suomalainen A, and Elo LL. Integrative omics approaches provide biological and clinical insights: examples from mitochondrial diseases. *J Clin Invest.* 2020;130(1):20-8.
28. Rahman J, and Rahman S. Mitochondrial medicine in the omics era. *Lancet.* 2018;391(10139):2560-74.
29. Sharma R, Reinstadler B, Engelstad K, Skinner OS, Stackowitz E, Haller RG, Clish CB, Pierce K, Walker MA, Fryer R, et al. Circulating markers of NADH-reductive stress correlate with mitochondrial disease severity. *J Clin Invest.* 2021;131(2).
30. Stewart JB, and Chinnery PF. The dynamics of mitochondrial DNA heteroplasmy: implications for human health and disease. *Nat Rev Genet.* 2015;16(9):530-42.
31. Koga Y, Akita Y, Nishioka J, Yatsuga S, Povalko N, Tanabe Y, Fujimoto S, and Matsuishi T. L-arginine improves the symptoms of strokelike episodes in MELAS. *Neurology.* 2005;64(4):710-2.
32. Rikimaru M, Ohsawa Y, Wolf AM, Nishimaki K, Ichimiya H, Kamimura N, Nishimatsu S, Ohta S, and Sunada Y. Taurine ameliorates impaired the mitochondrial function and prevents stroke-like episodes in patients with MELAS. *Intern Med.* 2012;51(24):3351-7.
33. Giannopoulos S, Samardzic K, Raymond BBA, Djordjevic SP, and Rodgers KJ. L-DOPA causes mitochondrial dysfunction in vitro: A novel mechanism of L-DOPA toxicity uncovered. *Int J Biochem Cell Biol.* 2019;117(105624.
34. Castillo J, Davalos A, and Noya M. Progression of ischaemic stroke and excitotoxic aminoacids. *Lancet.* 1997;349(9045):79-83.
35. Miladinovic T, Nashed MG, and Singh G. Overview of Glutamatergic Dysregulation in Central Pathologies. *Biomolecules.* 2015;5(4):3112-41.
36. DiFrancesco JC, Cooper JM, Lam A, Hart PE, Tremolizzo L, Ferrarese C, and Schapira AH. MELAS mitochondrial DNA mutation A3243G reduces glutamate transport in cybrids cell lines. *Exp Neurol.* 2008;212(1):152-6.

37. Sun X, Shi X, Lu L, Jiang Y, and Liu B. Stimulus-dependent neuronal cell responses in SH-SY5Y neuroblastoma cells. *Mol Med Rep.* 2016;13(3):2215-20.
38. Sun ZW, Zhang L, Zhu SJ, Chen WC, and Mei B. Excitotoxicity effects of glutamate on human neuroblastoma SH-SY5Y cells via oxidative damage. *Neurosci Bull.* 2010;26(1):8-16.
39. Picard M, Zhang J, Hancock S, Derbeneva O, Golhar R, Golik P, O'Hearn S, Levy S, Potluri P, Lvova M, et al. Progressive increase in mtDNA 3243A>G heteroplasmy causes abrupt transcriptional reprogramming. *Proc Natl Acad Sci U S A.* 2014;111(38):E4033-42.
40. Patgiri A, Skinner OS, Miyazaki Y, Schleifer G, Marutani E, Shah H, Sharma R, Goodman RP, To TL, Robert Bao X, et al. An engineered enzyme that targets circulating lactate to alleviate intracellular NADH:NAD(+) imbalance. *Nat Biotechnol.* 2020;38(3):309-13.
41. Lee CF, Caudal A, Abell L, Nagana Gowda GA, and Tian R. Targeting NAD(+) Metabolism as Interventions for Mitochondrial Disease. *Sci Rep.* 2019;9(1):3073.
42. Buzkova J, Nikkanen J, Ahola S, Hakonen AH, Sevastianova K, Hovinen T, Yki-Jarvinen H, Pietilainen KH, Lonnqvist T, Velagapudi V, et al. Metabolomes of mitochondrial diseases and inclusion body myositis patients: treatment targets and biomarkers. *EMBO Mol Med.* 2018;10(12).
43. Santra S, Gilkerson RW, Davidson M, and Schon EA. Ketogenic treatment reduces deleted mitochondrial DNAs in cultured human cells. *Ann Neurol.* 2004;56(5):662-9.
44. Hughes SD, Kanabus M, Anderson G, Hargreaves IP, Rutherford T, O'Donnell M, Cross JH, Rahman S, Eaton S, and Heales SJ. The ketogenic diet component decanoic acid increases mitochondrial citrate synthase and complex I activity in neuronal cells. *J Neurochem.* 2014;129(3):426-33.
45. Kanabus M, Fassone E, Hughes SD, Bilooei SF, Rutherford T, Donnell MO, Heales SJR, and Rahman S. The pleiotropic effects of decanoic acid treatment on mitochondrial function in fibroblasts from patients with complex I deficient Leigh syndrome. *J Inherit Metab Dis.* 2016;39(3):415-26.
46. Gibson GE, Starkov A, Blass JP, Ratan RR, and Beal MF. Cause and consequence: mitochondrial dysfunction initiates and propagates neuronal dysfunction, neuronal death and behavioral abnormalities in age-associated neurodegenerative diseases. *Biochim Biophys Acta.* 2010;1802(1):122-34.
47. Johnson SC, Kayser EB, Bornstein R, Stokes J, Bitto A, Park KY, Pan A, Sun G, Raftery D, Kaeberlein M, et al. Regional metabolic signatures in the Ndufs4(KO) mouse brain implicate defective glutamate/alpha-ketoglutarate metabolism in mitochondrial disease. *Mol Genet Metab.* 2020;130(2):118-32.
48. Ge YX, Shang B, Chen WZ, Lu Y, and Wang J. Adult-onset of mitochondrial myopathy, encephalopathy, lactic acidosis and stroke-like episodes (MELAS) syndrome with hypothyroidism and psychiatric disorders. *eNeurologicalSci.* 2017;6(16-20.
49. Kaufmann P, Engelstad K, Wei Y, Kulikova R, Oskoui M, Battista V, Koenigsberger DY, Pascual JM, Sano M, Hirano M, et al. Protean phenotypic features of the A3243G mitochondrial DNA mutation. *Arch Neurol.* 2009;66(1):85-91.
50. Hirata K, Akita Y, Povalko N, Nishioka J, Yatsuga S, Matsuishi T, and Koga Y. Effect of L-arginine on synaptosomal mitochondrial function. *Brain Dev.* 2008;30(4):238-45.
51. Kanellopoulos AK, Mariano V, Spinazzi M, Woo YJ, McLean C, Pech U, Li KW, Armstrong JD, Giangrande A, Callaerts P, et al. Aralar Sequesters GABA into Hyperactive Mitochondria, Causing Social Behavior Deficits. *Cell.* 2020;180(6):1178-97 e20.
52. Besse A, Wu P, Bruni F, Donti T, Graham BH, Craigen WJ, McFarland R, Moretti P, Lalani S, Scott KL, et al. The GABA transaminase, ABAT, is essential for mitochondrial nucleoside metabolism. *Cell Metab.* 2015;21(3):417-27.

53. Ahola-Erkkila S, Carroll CJ, Peltola-Mjosund K, Tulkki V, Mattila I, Seppanen-Laakso T, Oresic M, Tyynismaa H, and Suomalainen A. Ketogenic diet slows down mitochondrial myopathy progression in mice. *Hum Mol Genet.* 2010;19(10):1974-84.
54. Steele H, Gomez-Duran A, Pyle A, Hopton S, Newman J, Stefanetti RJ, Charman SJ, Parikh JD, He L, Viscomi C, et al. Metabolic effects of bezafibrate in mitochondrial disease. *EMBO Mol Med.* 2020;12(3):e11589.
55. Chao de la Barca JM, Simard G, Amati-Bonneau P, Safiedeen Z, Prunier-Mirebeau D, Chupin S, Gadras C, Tessier L, Gueguen N, Chevrollier A, et al. The metabolomic signature of Leber's hereditary optic neuropathy reveals endoplasmic reticulum stress. *Brain.* 2016;139(11):2864-76.
56. Bocca C, Kane MS, Veyrat-Durebex C, Chupin S, Alban J, Kouassi Nzoughet J, Le Mao M, Chao de la Barca JM, Amati-Bonneau P, Bonneau D, et al. The Metabolomic Bioenergetic Signature of Opa1-Disrupted Mouse Embryonic Fibroblasts Highlights Aspartate Deficiency. *Sci Rep.* 2018;8(1):11528.
57. Veyrat-Durebex C, Bocca C, Chupin S, Kouassi Nzoughet J, Simard G, Lenaers G, Reynier P, and Blasco H. Metabolomics and Lipidomics Profiling of a Combined Mitochondrial Plus Endoplasmic Reticulum Fraction of Human Fibroblasts: A Robust Tool for Clinical Studies. *J Proteome Res.* 2018;17(1):745-50.
58. Veyrat-Durebex C, Bris C, Codron P, Bocca C, Chupin S, Corcia P, Vourc'h P, Hergesheimer R, Cassereau J, Funalot B, et al. Metabo-lipidomics of Fibroblasts and Mitochondrial-Endoplasmic Reticulum Extracts from ALS Patients Shows Alterations in Purine, Pyrimidine, Energetic, and Phospholipid Metabolisms. *Mol Neurobiol.* 2019;56(8):5780-91.
59. Sumner LW, Amberg A, Barrett D, Beale MH, Beger R, Daykin CA, Fan TW, Fiehn O, Goodacre R, Griffin JL, et al. Proposed minimum reporting standards for chemical analysis Chemical Analysis Working Group (CAWG) Metabolomics Standards Initiative (MSI). *Metabolomics.* 2007;3(3):211-21.
60. Owen OE, Kalhan SC, and Hanson RW. The key role of anaplerosis and cataplerosis for citric acid cycle function. *J Biol Chem.* 2002;277(34):30409-12.
61. Smith ML, Baggerly KA, Bengtsson H, Ritchie ME, and Hansen KD. illuminaio: An open source IDAT parsing tool for Illumina microarrays. *F1000Res.* 2013;2(264.
62. Ritchie ME, Phipson B, Wu D, Hu Y, Law CW, Shi W, and Smyth GK. limma powers differential expression analyses for RNA-sequencing and microarray studies. *Nucleic Acids Res.* 2015;43(7):e47.
63. Robinson MD, McCarthy DJ, and Smyth GK. edgeR: a Bioconductor package for differential expression analysis of digital gene expression data. *Bioinformatics.* 2010;26(1):139-40.
64. Subramanian A, Tamayo P, Mootha VK, Mukherjee S, Ebert BL, Gillette MA, Paulovich A, Pomeroy SL, Golub TR, Lander ES, et al. Gene set enrichment analysis: a knowledge-based approach for interpreting genome-wide expression profiles. *Proc Natl Acad Sci U S A.* 2005;102(43):15545-50.